Journal of Applied Polymer Science

Determination of Highly Porous Plastic Foam Structural Characteristics by Processing Light Microscopy Images Data

Ilze Beverte
Institute of Polymer Mechanics, University of Latvia, Aizkraukles Street 23, LV1006, Riga, Latvia
Correspondence to: I. Beverte (E-mail: ilzebeverte@edi.lv)

ABSTRACT: Mathematical modelling of physical and mechanical properties of plastic foam as well as numerous practical applications requires knowledge of foam structural characteristics. A necessity exists to determine the characteristics of the spatial structure of inhomogeneous materials comprising inclusions of other material, e.g., polyurethane foam without destructing the material and analysis of each element. A methodology is elaborated for preparing highly porous plastic foam specimens and investigation of foam strut-like structure with light microscopy (LM) by taking images in three mutually perpendicular planes. A mathematical model is developed for highly porous plastic foam for the determination of probability density functions of its building elements—polymeric struts': (a) length and (b) angles, using LM images in three mutually perpendicular planes. Computer codes are created and parameters of distribution functions for strut's length and angles are calculated using experimental data for verification. A good correspondence of the modelling results with experimental data is proved to exist. © 2013 Wiley Periodicals, Inc. J. Appl. Polym. Sci. **2014**, *131*, 39477.

KEYWORDS: foams; microscopy; structure-property relations; mechanical properties; polyurethanes

Received 18 February 2013; accepted 24 April 2013
DOI: 10.1002/app.39477

INTRODUCTION

Symmetry of physical and mechanical properties of materials is connected to symmetry of their structure, e.g. free-rise plastic foam with regard to elasticity and strength are transtropic composite materials (polymer and gaseous phase) with the plane of isotropy perpendicular to the foam rise direction (RD). Mathematical modelling of physical and mechanical properties of foam materials as well as numerous practical applications requires knowledge about their structure. A necessity exists to determine the characteristics of the actual spatial structure of inhomogeneous materials (Porous ceramics, porous plastics, fibers' reinforced concrete, human bone tissues, etc.) comprising inclusions of other material (Gas bubbles, metal beads, short metal fibers, irregular silica particles, etc.) without destructing the material and analysis of each element.

Two major cases can be distinguished for plastic foam, e.g. polyisocyanurate (PIR) and polyurethane (PUR) with regard to structure: (1) low porosity $P < 30\%$, when the foam structure is formed by un-interconnecting gas bubbles and distribution of bubbles' diameters has to be determined and (2) high porosity $P > 90\%$, when the foam structure is formed by a framework of polymeric struts connected in nodes.[1–3] Only highly porous foams are considered further where the polymeric struts are the main load-carrying elements.

The experimental studies on plastic foam cellular structure often deal with the cell's diameters' projections, measured from images in directions parallel and perpendicular to rise direction. Histograms of cell's principal diameters' projections d^p_1, d^p_2, and d^p_3 on three image planes, determined with the help of light microscope (LM) or scanning electron microscope (SEM), were presented in Refs. 2,4. A nonlinear relationship between moduli of elasticity E_1, E_2, and E_3 and elongation degrees K of the cells $K_1 = d^p_3/d^p_1$ and $K_2 = d^p_3/d^p_2$ was derived. Frequency of cells elongation degrees in free-rise blocks of PUR and PVC foams as a function of block's thickness coordinate was investigated from LM images.[2] It was found that in the middle of a PVC block the cells tend to be nearly spherical and have K_1, $K_2 \approx 2$ at the bottom and top of the block.

An investigation was performed on the relationships between cell morphology, density, and mechanical properties in transtropic PUR materials moulded in cylindrical moulds.[4] Three mould sizes were used to study changes in cell morphology (Projections of cell area, cell diameter, aspect ratio, cell angle, cell edge length, cell face thickness, and cell edge thickness on SEM image plane), density, and mechanical properties (Young's modulus and collapse stress) with respect to position within the mould. The mean cell diameter's projection was determined from SEM images as average length of diameter measured at 2 degrees increment. The density, closely linked to structural

characteristics was shown to increase from the top to the bottom of the reference mould but did not change significantly in the small and tall moulds.

The mercury absorption test was used to determine frequency of actual pores' diameters in highly porous closed-cell PUR foam.[1] The corresponding histograms were markedly asymmetric with the maximum shifted to the smaller diameters' values. The method was reported as not suited for open cell foam structure characterising. For better understanding of the foaming nature of highly porous foam the frequency of bubbles radii in low and average porosity foam $P = 30–70\%$ was determined and was reported to be asymmetric as well with the maximum, shifted to the smaller radii values.[5,6] Modelling of distribution functions of bubbles' radii from circles' radii distribution on the sample's cross section was undertaken.

Structural characteristics such as the mean cell strut thickness, cell size, and their standard deviations were obtained by the nondestructive X-ray tomography, using the Phoenix Nanotom.[7] The nano-tom produced X-rays by accelerating electrons that hit a target material. During a measurement, a specimen rotated while it was exposed to X-rays. The projections made, were combined to generate a reconstruction of the volume of the specimen, which resulted in a high 3D resolution image of the specimen. The high resolution image was then analyzed with image processing software to obtain properties like the mean cell size, the mean cell strut thickness and their standard deviations. Within that investigation the software developed by Scanco Medical AG was used. The results were obtained only for closed-cell foam.

A certain similarity exists in investigation of fiber architecture in short fiber-reinforced polymer composite foam and determination of struts spatial distribution characteristics.[8] A nondestructive X-ray imaging technique was used to determine the internal structure in a phenolic polymer foam reinforced with short glass fibers. The computerized tomography was used to measure the fiber length distribution and orientation distribution, the two parameters that are critical to the behavior of short-fiber reinforced composites.

The Theoretical Studies

In one of the first theoretical models of plastic foam, a combined strut-node element was implemented.[9] Struts were distributed randomly in the space and their amount in a spatial angle was calculated based on the total amount of struts in a unit volume. Only isotropic structure was considered assuming that the struts were distributed randomly. Similar approach was used in Ref. 10. Structural units comprising a strut and an air sheath were modelling the structure in Ref. 11, where an angular distribution function was modelling the structural anisotropy. The orientation of a structural unit with respect to the foam coordinate frame of reference was defined by the parameter θ, where θ was the angle between the foam principal axis O3 (parallel to the foam rise direction) and the unit's axis O3 (parallel to the longitudinal axis of a strut). The overall foam modulus could be estimated for an angular distribution of structural units by mechanically coupling such a distribution with a continuity of stress (Reuss average) or a continuity of strain (Voigt average). For a random aggregate, the Reuss and Voigt values lead to lower and upper bounds respectively.

Modelling of plastic foam structure rely widely on applying a certain geometrical figure (Space filling or un-filling) as a model cell: a cube, a hexagonal prism, a truncated cone, a tetrakaidecahedron, a pentagon dodecahedron, an ellipsoid, etc.[1–3] The porosity P of the foam is assigned to the model cell and the dimensions of elements (Struts, nodes, and faces) are calculated from geometrical considerations. The approach neglects the statistical distribution over the main characteristics of structural elements: length, width, spatial orientation, etc.

In Ref. 12 a structural model was proposed combining the two mentioned approaches: (1) a model cell and (2) orientational averaging. The model cell was considered in the shape of a sphere or an ellipsoid built around a node with $N = 2, 3, \ldots,$ 10 evenly distributed struts emerging from it. To model the spatial orientations, the strut system was rotated as a whole around the node over three Euler's angles φ_E, ψ_E, and θ_E. Transtropy was implemented by a linear coordinates' transformation along foam rise direction. Histograms of struts' length distribution were calculated for the obtained sample of N struts and found to be asymmetric, with a maximum shifted to the smaller values.

The Voronoi tessellation technique and the finite element method were utilized to investigate the microstructure–property relations of three-dimensional cellular solids (foams) that had irregular cell shapes and nonuniform strut cross-sectional areas (SCSAs).[13] Perturbations were introduced to a regular packing of seeds to generate a spatially periodic Voronoi diagram with different degrees of cell shape irregularity and to the constant SCSA to generate a uniform distribution of SCSAs with different degrees of SCSA nonuniformity. The analysis was based on a reference cell—tetrakaidecahedron (Kelvin cell).

In Refs. 14,15 the foam structure was represented by a sample of struts that was obtained by turning a single strut in space to undergo all spatial orientations. A model was presented for calculating the linear elastic constants of highly porous plastics having a strut-like structure by orientational averaging the rigidity tensor of a structural element consisting of an gas sheath and a load-carrying element in the form of a straight strut with a piecewise constant cross section. The nonuniform orientational distribution of the elements was also taken into account.

Methods of statistical geometry are used for microstructural modelling and analysis of crystals, metal melts, minerals, suspensions. etc. The calculations lead to Gamma-functions and analytical solutions can be found mainly for special cases, e.g. even, increasing, decreasing, or triangular probability density functions.[1]

Reasons for Undertaking the Research

Both the experimental and theoretical methods comprise several drawbacks. The fact that length' and angles' projections are determined from images and used as input data for struts' length and angles in further modelling is mainly neglected. The X-ray-based simulation requires availability of a nano-tome of a sufficient capacity and does not provide deeper understanding

Table I. Mechanical Properties of PUR Foam in Compression

		Block				
N	Characte-ristics	1	2	3	4	5
1	Parallel to OX_1					
	ρ_f (kg m^{-3})	33.2	37.4	54.6	81.0	75.0
		±0.0	±1.3	±0.3	±0.5	±0.3
		0 (%)	3 (%)	1 (%)	1 (%)	0 (%)
	E_1 (MPa)[a]	4.2	5.7	9.4	18.9	22.9
		±0.2	±0.3	±0.3	±1.7	±2.8
		5 (%)	6 (%)	3 (%)	9 (%)	13 (%)
2	Parallel to OX_2					
	ρ_f (kg m^{-3})	32.7	33.6	49.2	76.4	75.1
		±0.2	±0.4	±0.1	±0.2	±1.8
		1 (%)	1 (%)	0 (%)	0 (%)	2 (%)
	E_2 (MPa)[a]	4.5	5.3	11.3	19.2	21.4
		±0.2	±0.2	±0.9	±2.5	±2.7
		4 (%)	4 (%)	8 (%)	13 (%)	13 (%)
3	Parallel to OX_3					
	ρ_f (kg m^{-3})	33.1	38.5	54.4	80.3	74.0
		±0.2	±0.3	±0.2	±0.3	±1.2
		1 (%)	1 (%)	0 (%)	0 (%)	2 (%)
	E_3 (MPa)[a]	10.5	7.5	20.1	26.5	31.5
		±0.5	±0.1	±0.3	±1.1	±1.2
		4 (%)	1 (%)	2 (%)	4 (%)	4 (%)
	E_3/E_1	2.47	1.32	2.14	1.40	1.43
	E_3/E_2	2.33	1.40	1.77	1.38	1.47
	Average $E_3/E_{1,2}$	2.40	1.36	1.95	1.39	1.45
	Place in $E_3/E_{1,}2$ range	5	1	4	2	3

[a] Moduli E_1, E_2, and E_3 were calculated at $\varepsilon_{ii} \approx 2\%$, $ii = 1$, 2 and 3.

of structure to model different elongation degrees of foam cells. The theoretical approaches often rely on artificial regularization of the structure. The models based on orientational averaging are using angular distribution functions of length and angles that are not verified experimentally because of the lacking of corresponding data. No investigations are known to the author developing methods for the determination of the probability distribution of the actual dimensions and spatial orientation angles of struts from LM, SEM, or other images. Therefore experiments were performed and a mathematical model and several computational codes were developed for highly porous PUR foam, permitting to determine probability density functions of polymeric struts': (a) length and (b) spatial orientation angles, using experimental data from the images obtained by a penetrating light LM.

EXPERIMENTAL

The generalized Neumann's principle determines that the symmetry of structure of a material cannot be higher than symmetry of any of its physical properties. To estimate the mode of mechanical anisotropy, the average Young's moduli E_i, i, $j = 1$, 2, and 3 in compression, standard deviations and coefficients of variation were determined, Table I for five industrially manufactured free-rise in a mould (RD parallel to OX_3, Figure 1) PUR foam blocks with average densities $\rho_f = 33$, 37, 53, 79, and 75 kg m^{-3} and porosity $P > 90\%$, $P = 1 - \rho_f/\rho_{pob}$ where ρ_f and ρ_{pol} are densities of foam and monolithic polymer. The outer crust of the blocks was removed to retain homogeneous material with final dimensions 50 × 50 × 20 cm. The samples were rectangular prisms 100 × 50 × 50 mm, strain rate $\varepsilon' = 10\%\text{min}^{-1}$, temperature $T = +18°\text{C}$. Four samples, cut out from the bottom half (with regard to the height) of the blocks, were tested for each point. The technical performance of tests was similar to that presented by the author in Ref. 16.

As $E_3 > E_1 \approx E_2$, material can be considered as transtropic with regard to mechanical properties. As symmetry of mechanical properties is linked to symmetry of structure, transtropic structure can be expected and investigations were planned in a corresponding way.

Microscopy

A column 20 × 2.5 × 2.5 cm, height parallel to RD, was cut out from each block. The column was situated in the geometrical center of the blocks' plane X_1OX_2 to minimize possible

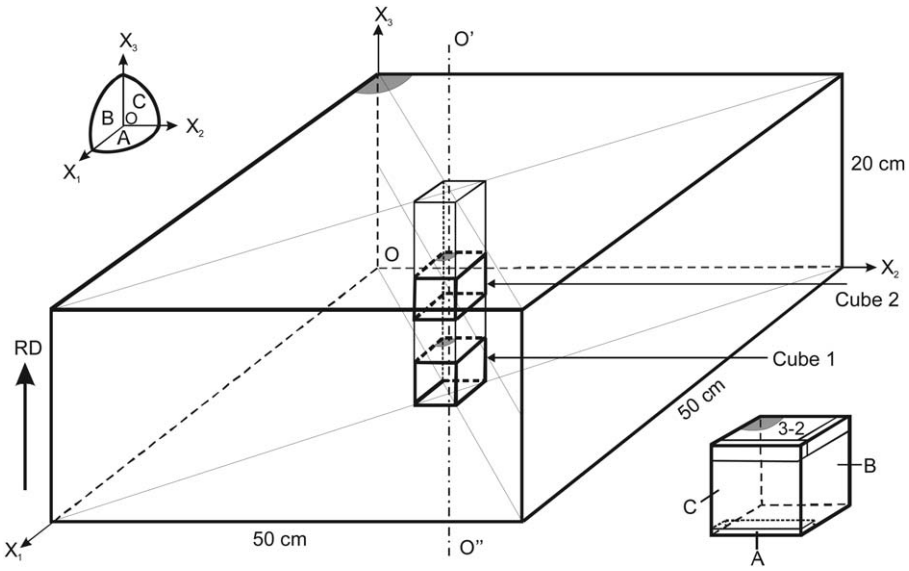

Figure 1. Cubes 1 and 2 in a free-rise foam block.

influence of anisotropy because of contact with mould sides, Figure 1. Two cubes 2.5 × 2.5 × 2.5 cm were cut out from each column. Cube 1 was located on the bottom of the column/block, cube 2 in the center of the column/block, difference in the coordinates X_3 of centers of cubes $\Delta X_3 = 8.75$ cm. A mark on the far left top corner of the blocks, columns and cubes was made to avoid unintended turns around OX_3.

An experimental specimen 0.5 × 5 × 25 mm was cut from the sides A, B, and C (X_3 = const., X_2 = const. and X_1 = const., where X_1, X_2, and X_3 are foam principal symmetry axes) of a cube (Figure 1) and attached to a glass slide. Light beams from two external sources were directed to the specimen: (1) parallel to the plane of specimen and (2) in angle ≈ 30° with the vertical axis OX_3. 3 × 2 = 6 images (1024 × 768), 55×, were taken by a digital camera (DC; 4 mpx), attached to the LM for each block as well as an image of a 1-mm-long calibrating size. The focus of the LM was fixed on the upper struts of the surface. The approximate depth of focus range was $h_F \approx 0.35 \pm 0.05$ mm.

Elements on the images are projections of the actual (a) dimensions of foam structural elements struts, nodes, and faces on the image planes A, B, or C and (b) angles formed by the struts with different axes. L^P_A, L^P_B, and L^P_C are projections of a strut's length L on images with planes parallel to A, B, and C; φ^P, θ^P_B, and θ^P_C are projections of a strut's spherical angles φ and θ on images with planes parallel to A, B, and C. Projections were measured from printed images, taking into account the corresponding image files on PC display simultaneously.

Measurements from LM Images

Image areas corresponding with the general character of an image were chosen for determination of the struts' length projections. Length projections were measured with a ruler, precision ± 0.5 mm; angles were measured with a protractor, precision ± 1°. Application of a certain image processing software was tested, but turned out to be less useful for the purpose. It was important for the observer to consider all elements one by one in the chosen area of the image. Only obvious defects (Local angular orientation of a group of struts differing from dominating orientation, untypically shaped struts, clusters of base polymer forming untypical nodes, etc.), not corresponding with the general character of the projections were omitted. A subjective tendency of an observer to: (a) to choose longer projections and (b) not to notice/include very short projections was recognized and constantly corrected. At the same time a short projection could correspond to (a) a short strut having angle $\beta_1 \approx 0°$ with the image plane or to (b) a long strut having $\beta_2 \approx 90°$ with the image plane, Figure 2.

As the foam in blocks 4 and 5 had densities 1.5–2 times higher than foam in blocks 1, 2, and 3, their structural elements struts and their projections visible on the images were smaller. To reduce potential subjective error of the observer, choosing projections and measuring them, the images of foam 4 and 5 were

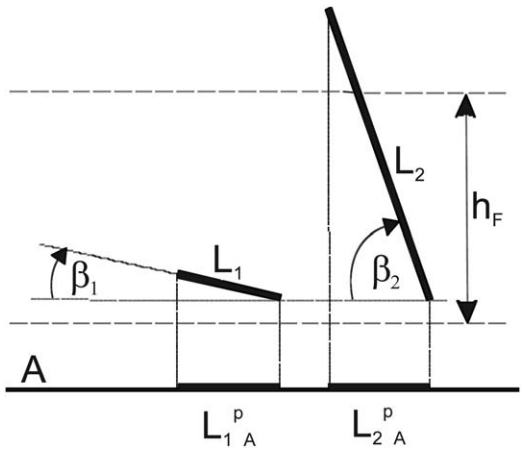

Figure 2. Projections of struts' L_1 and L_2 on image plane A.

Table II. Experimental Data of Struts' Projections

			Image A			Images B + C					
Specimen	Image	N	L^p_{Amax} (unit)	L^p_{Amod} (unit)	$l^{mod}{}_A$	L^p_{BCmax} (unit)	L^p_{BCmod} (unit)	$l^{mod}{}_{BC}$	L^p_{Aaver}; L^p_{BCaver}, (unit)	s, (unit)	v (%)
1-1	11A	300	11.0	1.5	2	-	-	-	3.7	2.3	63
	11B+11C	300	-	-	-	18.0	4.5	5	6.4	4.1	64
1-2	12A	100	11.5	2.5	3	-	-	-	4.2	2.6	63
	12B+12C	200	-	-	-	18.0	4.5	5	7.3	4.0	55
2-1	21A	100	13.0	2.5	3	-	-	-	4.8	2.7	57
	21B+21C	200	-	-	-	19.0	4.0	4	6.6	3.7	56
2-2	22A	100	12.0	2.5	3	-	-	-	5.1	2.8	54
	22B+22C	200	-	-	-	15.0	4.0	4	6.1	3.4	55
3-1	31A	100	7.0	1.5	2	-	-	-	2.7	1.4	53
	31B+31C	200	-	-	-	12.0	2.5	3	4.2	2.0	46
3-2	32A	100	8.0	2.5	3	-	-	-	3.0	1.6	51
	32B+32C	200	-	-	-	11.5	2.5	3	4.3	2.2	52
4-1	41A	100	6.0	1.5	2	-	-	-	2.2	1.2	55
	41B+41C	200	-	-	-	8.5	2.5	2	2.9	1.7	59
4-2	42A	200	8.2	2.5	3	-	-	-	2.5	1.4	55
	42B+42C	200	-	-	-	7.8	2.5	3	2.6	1.4	55
5-1	51A	100	6.0	1.5	2	-	-	-	2.2	1.3	58
	51B+51C	200	-	-	-	10.6	2.5	3	3.2	2.2	68
5-2	52A	100	6.4	2.5	3	-	-	-	2.4	1.3	55
	52B+52C	200	-	-	-	8.5	2.5	2	3.2	1.8	55

printed in an enlarged scale (141%) to maintain app. equal conditions for the observer. A certain insufficiency of short projections L^p of struts length $0 < L^p \leq 1$ unit (1 mm on printed images was denoted as 1 unit; scale 1 unit = 1:55 mm) was observed on the images A of specimens from 3, 4, and 5 blocks, $\rho_f > 49$ kg m^{-3} possibly because of the merging of short struts into clusters of base polymer.

A representative layer of foam was defined as a layer having thickness equal to the depth of focus range h_f. It was assumed that the character of struts in the representative layer corresponds to their average character in foam cubical specimens. Principles for including strut's length projections into the representative statistical sample were formulated:

1. Only projections having both ends visible were considered for including in the representative sample. It was important for the observer to estimate properly how far reached the strut while entering the node for each foam density.
2. Only projections depicted sharply along their whole length or along a certain part of the length were included in the sample. Elements with changing sharpness along length correspond to struts situated angularly to the image plane and having length reaching outside the representative layer. The number of such elements was divided by 2 for each group of length, since they belong to two representative foam layers.
3. Blur elements were considered to be outside (above or beyond) the representative layer and as such were not included into the sample.

The struts' length L, projections L^p, angles θ, φ, and projections θ^p and φ^p are continuous random variables. The number N of elements in the representative statistical sample, necessary for a sufficiently precise finding of the fitting theoretical probability density function (the smoothing function) was determined. For majority of A images $N = 100$. Because of foam transtropy the values of projections measured from images C and B, were merged into a statistical sample B + C = BC of $N = 200$ elements. Were the character of the distribution remained unclear, number of elements was increased up to $N = 300$. The scale was not yet taken into account for convenience of operating with images.

Values of projections L^p in a statistical sample were sorted and arranged into I = ROUNDUP($L^p{}_{max}$) number of classes, where ROUNDUP($L^p{}_{max}$) was the value of the biggest projection $L^p{}_{max}$ in the sample rounded up to the nearest biggest integer value. The scale 141% was taken into account for foam 3 and 4 prior to that. Class width $h = 1$ unit,

$$(i-1)\,h < L^{pi}_k \leq i\,h,\ i=1,2,\ldots,I,\ k=1,2,\ldots,K^i, \qquad (1)$$

where K^i – number of elements in the i-th class. Modes $L^p{}_{Amod}$ and $L^p{}_{BCmod}$ of samples $L^p{}_{An}$, $L^p{}_{BCn}$, $n = 1, 2, \ldots, N$, were determined as central numbers of the modal class, where $L^p{}_{An}$, $L^p{}_{BCn}$

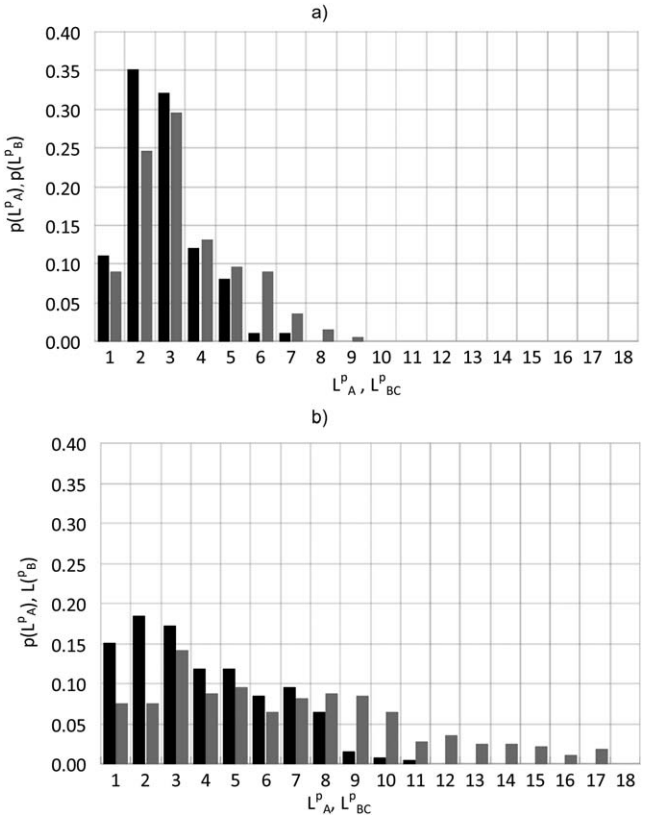

Figure 3. Distribution of L^P_A (black) and L^P_{BC} (grey) of the experimental specimens: (a) 4-2 with the most equal statistical samples of length projections in planes A and B (or C) and (b) 1-1 with the most differing statistical samples of length projections in planes A and B (or C).

- projections of L_n on planes A, B, and C, I^{mod}—the number of the modal class. The first initial and the second central moment (Mean—the average value L^P_{aver} and the standard deviation s) and coefficient of variation v were calculated for statistical sample of struts of each experimental specimen, Table II.[17,18] Class width = 1 unit.

Histograms of probabilities $p(L^P_i)$, $i = 1, 2, \ldots, I$ for L^P_A and L^P_{BC} were constructed, Figure 3. The asymmetric histograms had a tail extending to the right and a mode at L_{mod1}. Around 85% of histograms had a second mode at $L^P_{\text{mod2}} > L_{\text{mod1}}$, $p(L^P_{\text{mod2}}) < p(L^P_{\text{mod1}})$. The presence of the second mode could be explained by a certain close order of the gas bubbles in the liquid phase and a subsequent regularization of the system of cells and struts. SEM and LEM investigations approved that the majority of cells were shaped like tetrakaidecahedrons or pentagon dodecahedrons.

For low porosity ($P < 30\%$) isotropic foam the asymmetric variation series of radii R of un-interconnecting circles on the samples' cutting surface are often smoothed with a probability density function in the mode of a power law with an exponential cutoff[1]:

$$f(R, q, \alpha, b) = R^q \exp(-\alpha R^b);\ R > 0;\ q, \alpha, \text{ and } b > 0;\ f(R, q, \alpha, b) \geq 0. \quad (2)$$

After normaliszation for the total length range of radii R:

$$f(R, q, \alpha, b) = AR^q \exp(-\alpha R^b);\ A = 1/\int_{-\infty}^{\infty} f(R, q, \alpha, b)dR, \quad (3)$$

where A is the normalization factor; q, α, and b the parameters determining sharpness of maximum and asymmetry. As the histograms of experimental values of projections L^P_A and L^P_{BC} were found to be asymmetric and had a maximum shifted to the smaller values, the same mode of function was chosen for smoothing:

$$f(L^p, q, \alpha, b) = A(L^p)^q \exp\{-\alpha(L^p)^b\};\ L^p > 0;\ q, \alpha, \text{ and } b > 0;\ f(L^p, q, \alpha, b) \geq 0 \quad \text{and} \quad A = 1/\int_{-\infty}^{\infty} f(L^p, q, \alpha, b)dL^p. \quad (4)$$

The theoretical probability was calculated:

$$\Delta p(L^p_i) = f(L^p_i)\, h,\ h = 1.0 \text{ unit},\ \Delta p(L^p_i) \approx p\{L^p_{i-1} < L^p \leq L^p_{i-1} + h\},\ i = 1, 2, \ldots, I \quad (5)$$

where L^P_i is the biggest value in the i-th class; $L^P_0 = 0$. The values of q and were fixed as $q = 1.0$, $b = 1.5$ in order to have one parameter α and more obvious comparison of trends of different cases. Numerical analysis revealed that α values varied in the limits $0.02 \leq \alpha \leq 0.35$ were appropriate to find the best fitting theoretical functions for the experimental statistical samples. According to the method of moments, the parameter α, providing the least difference between L^P_{aver} of the experimental (E) and theoretical (T) data samples, was defined as the characteristic parameter of the best fitting theoretical probability density function $f(L^P, \alpha)$:

$$IL^p_{\text{aver}}{}^E - L^p_{\text{aver}}{}^T I \leq \varepsilon, \text{ where } \varepsilon \text{ is the precision.} \quad (6)$$

The function $f(L^P, \alpha)$ comprises one parameter α therefore only equality of one kind of moments—the means was required. Numerical calculation results were presented in Table III. Parameters α corresponding to probability density distribution functions of struts' length projections on experimental images A, B, and C were denoted as $\alpha^P{}_A{}^E$ and $\alpha^P{}_{BC}{}^E$ and their difference $\Delta\alpha^{pE} = \alpha^P{}_A{}^E - \alpha^P{}_{BC}{}^E$. To characterize the anisotropy of foam blocks, anisotropy degree K_3 was implemented as $K_3 = \alpha^P{}_A{}^E / \alpha^P{}_{BC}{}^E$, $K_3 = 1.0$ for isotropic foam. Gradient of anisotropy in a foam block is characterized by $\Delta K_3 = K_3{}^2 - K_3{}^1$, where $K_3{}^1$ and $K_3{}^2$ are anisotropy degrees of the bottom experimental specimens 1 and center specimens 2.

As both the type and parameter of function $f(L^P, \alpha)$ are known, the hypothesis of fitting between the probability determined by experimental histograms $F^E(x)$ and theoretical smoothing probability distribution functions $F^T(x)$ was evaluated according to Kolmogorov's criterion [19]:

$$D_n = \max|F^E(x) - F^T(x)| \text{ and } D_n\sqrt{N} \geq \lambda, \quad (7)$$

where N is the number of elements in the statistical sample. For majority of experimental specimens considered, the quantity $\lambda \leq 0.70$ and $P(\lambda) \geq 0.711$ that corresponds to a good fitting, where $P(\lambda)$ is a tabulated probability for $0.0 \leq \lambda \leq 2.0$.[19] It was

Table III. Parameters of the Theoretical Distribution Functions Smoothing the Experimentally Determined Histograms of Struts' Projections

Block	Speci-men	$\alpha^{p}{}_{A}{}^{E}$	$\alpha^{p}{}_{BC}{}^{E}$	$\Delta\alpha$	K_3	ΔK_3	K_3^{aver}	Place in K_3^{aver} range
1	1-1	0.15	0.06	0.09	2.50	0.10	2.45	5
	1-2	0.12	0.05	0.07	2.40			
2	2-1	0.13	0.09	0.04	1.44	0.32	1.28	2
	2-2	0.09	0.08	0.01	1.13			
3	3-1	0.31	0.16	0.15	1.94	0.17	1.85	4
	3-2	0.23	0.13	0.10	1.77			
4	4-1	0.31	0.22	0.09	1.41	0.33	1.24	1
	4-2	0.27	0.25	0.02	1.08			
5	5-1	0.29	0.18	0.11	1.61	0.16	1.53	3
	5-2	0.29	0.20	0.09	1.45			

concluded that foam in cubes 2 were more isotropic ($\Delta\alpha^2 < \Delta\alpha^1$) than in cubes 1, as they were located closer to the top of the free-rise block. That corresponded with the experimental results reported in Refs. 1–3. To characterize the macroscopic properties of the foam block, average anisotropy degree was implemented as $K_3^{aver} = (K_3^1 + K_3^2)/2$. The value of K_3^{aver} was the smallest for block 4: $K_3^{aver} \approx 1.24$ and the biggest for block 1: $K_3^{aver} \approx 2.45$. LM images of (1) the most isotropic experimental specimen 4-2 and (2) the most transtropic one 1-1 were presented in Figures 4 and 5.

A correspondence exists between the anisotropy mode displayed by mechanical properties, Table I and anisotropy of structure, Table III.

THEORETICAL

Mathematical Modelling

Free-rise highly porous ($P > 90\%$) foam produced in an open mould having dimensions l_1, l_2, and l_3 along axis OX_1, OX_2, and OX_3 were considered. Several cases of the foam structural anisotropy can arise in dependence of mutual proportions of mould's dimensions, Table IV. Elongation of cells in the foam volume because of relatively big height of mould $l_{31} = l_3/l_1 >> 1$ and $l_{32} = l_3/l_2 >> 1$ had to be distinguished from local elongation of cells in the outer crust of a block or because of contact with mould.[1–3]

The structure of foam can be characterized by probability density functions of the struts': (1) length L and (2) spherical coordinates φ and θ, Figure 6, therefore mathematical modelling of foam structure was performed in several stages.

Struts' Spatial Distribution in Isotropic Foam

In isotropic foam the statistical samples of the struts' length projections on planes A, B, and C are similar. Then it can be assumed that struts are distributed spatially evenly and a certain spatial angle $d\omega$ corresponds to each strut, $d\omega$ being measured by the corresponding square dS on the spherical surface, Figure 6.

In the mathematical model the struts are considered to emerge from the center O of a sphere, radius L, the direction of the i-th strut being defined by spherical coordinates φ_i and θ_i, then $d\omega = dS/L^2$. It was assumed that the spatially even distribution of struts' could be achieved by an even distribution of the equal elementary squares dS_0 (Corresponding to a single strut), on the surface of the sphere, center of a square being intersection of the strut with sphere surface.

To determine arrays φ_i and θ_i of all spatially evenly distributed struts', the sphere surface was divided into bands by steps $d\theta$ = constant along angle θ, starting from the equatorial plane X_1OX_2. The spherical coordinates of the bottom

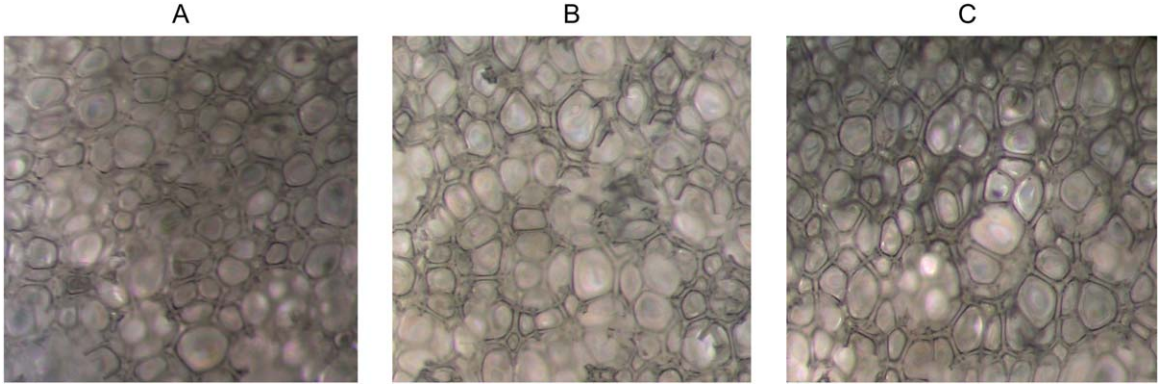

Figure 4. LM images of the experimental specimen 4-2, $K_3 = 1.08$, $\rho_f = 79$ kg m^{-3}, RD ↑for images B and C. [Color figure can be viewed in the online issue, which is available at wileyonlinelibrary.com.]

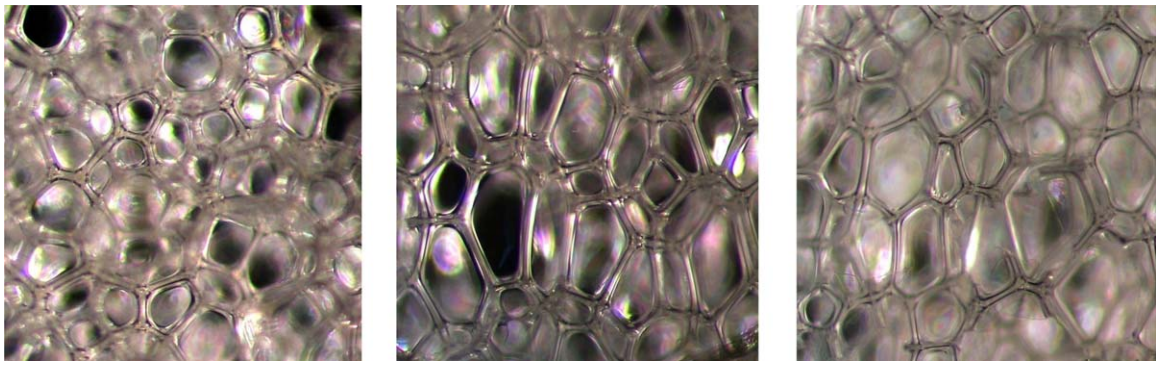

Figure 5. LM images of the experimental specimen 1-1, $K_3 = 2.50$, $\rho_f = 33$ kg m^{-3}, RD ↑for images B and C. [Color figure can be viewed in the online issue, which is available at wileyonlinelibrary.com.]

Table IV. Anisotropy Modes in Dependence of Mould's Dimensions

			Spatial distribution	
N	Proportion	Anisotropy	φ	θ
1	$l_2 > l_1, l_3 >> l_1, l_2$	Orthotropy	$f_1(\varphi)$	$f_2(\theta)$
2	$l_1 \approx l_2, l_3 >> l_1, l_2$	Transversel isotropy (Transtropy)	Even	$f(\theta)$
3	$l_1 \approx l_2 \approx l_3$	Isotropy	Even	Even

(b) and top (t) edges and parallel to them central line of the k-th band equal to

$$\Theta_k^b = \pi/2 - k\,d\theta,\ \theta_k^t = \pi/2 - (k-1)\,d\theta \text{ and } \theta_k^C = \pi/2 - (k+1/2)\,d\theta. \tag{8}$$

As symmetry exists along the octants of coordinate system $X_1OX_2X_3$ only the first octant (Quarter bands instead of circular bands) were considered for calculations of φ_i and θ_i:

$$0 \le \varphi < \pi/2,\ 0 \le \theta \le \pi/2. \tag{9}$$

Each k-th quarter band had to be divided into elementary squares by steps $d\varphi_k$ along φ, starting from the positive half-axis OX_1. The area S_1 of the first quarter band is $S_1 = 1/4\ (2\pi Lh)$, where h is the height of the band. Then

$$S_1 = 1/4\,(2\pi L^2 \sin\, d\theta) = 1/2\,\pi L^2 \sin\, d\theta \approx 1/2\,\pi\, L^2 d\theta. \tag{10}$$

For the first quarter band it was assumed $d\varphi_1 = d\theta$ then number N_1 of elementary squares in the first quarter band is

$$N_1 = \pi/(2\,d\varphi), \tag{11}$$

and area of an elementary square equals to

$$dS_0 = dS_{01} = S_1/N_1 = L^2 d\theta\, d\varphi. \tag{12}$$

The area of the k-th quarter band is $S_k = 1/4\ (2\pi Lh_k)$, where h_k is the height of band:

$$h_k = L(\sin(kd\theta) - \sin((k-1)d\theta)),\ k = 1, 2, \ldots, \pi/(2d\theta), \text{ then} \tag{13}$$

$$S_k = 1/2\,(2\pi L^2(\sin(kd\theta) - \sin((k-1)d\theta))). \tag{14}$$

The key assumption of the proposed model was keeping the area of elementary squares in all bands constant: $dS_{0k} = dS_0 =$ const. As area S_k of the bands is changing (Decreasing with θ_k increasing) it was impossible to perform a precise division of a

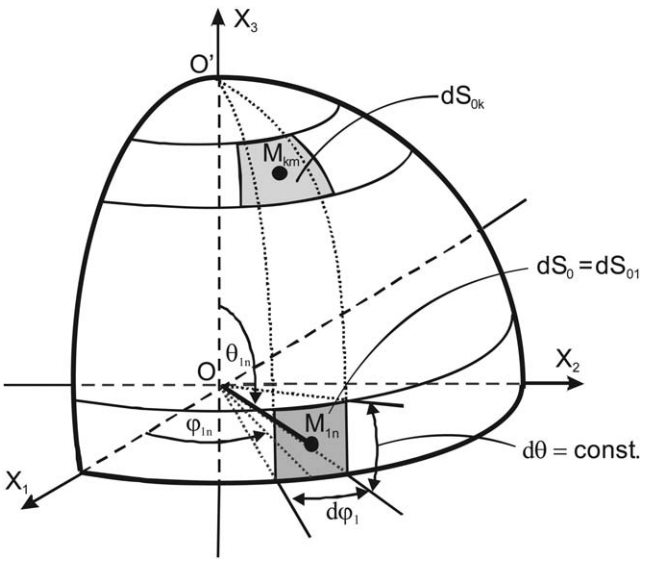

Figure 6. Elementary squares dS_{01} and dS_{0k}, corresponding to a single strut OM_{1n} and OM_{km} of the first and the k-th bands.

band (Besides the first one, $k = 1$) into squares dS_0 because of a residue, remaining. Therefore an approximate number of squares dS_0 in the k-th band was calculated first:

$$n_k = S_k/dS_0 = \pi L^2 ((\sin(kd\theta) - \sin((k-1)d\theta))/ (L^2 d\theta\, d\varphi),\ k = 1, 2, \ldots, \pi/(2d\theta). \quad (15)$$

Value of n_k was rounded to the nearest integer n'_k and value of dS_{0k} was recalculated for the k-th band:

$$dS_{0k} = S_k/n'_k. \quad (16)$$

Because of this the step along φ for the k-th band had to be recalculated, too:

$$d\varphi_k{}' = \pi/(2n'_k),\ d\varphi k' = \text{constant for } k = \text{constant} \quad (17)$$

For each unevenly numbered band (1, 3, …) the first strut is placed in the plane $X_2 = 0$, i.e. the first step along φ is a half-step $d\varphi_k/2$ to provide more even distribution of elementary squares. To estimate the precision of division into elementary squares, the relative difference between dS_0 and dS_{0k} was calculated for each band:

$$\Delta S_{0k} = (dS_0 - dS_{0k})/dS_0,\ k = 1, 2, \ldots, \pi/(2d\theta). \quad (18)$$

When the value of ΔS_{0k} became higher than the precision set *a priori*, the elementary squares dS_0k were calculated from ring bands $0 \le \varphi < 2\pi$ instead of quarter bands. That permitted to retain the necessary precision for dS_{0k}.

Finally θ_k of all struts in the k-th quarter band were calculated as coordinates of the center (intersection of diagonals) of the corresponding elementary square dS_{0k}:

$$\theta_k = \theta_k^C = \pi/2 - (k+1/2)\, d\theta,\ k = 1, 2, \ldots, \pi/(2d\theta). \quad (19)$$

The coordinate φ_{kn} of the n-th strut in the k-th quarter band was calculated:

$$\varphi_{kn} = (1/2+i)\, d\varphi_k{}',\ n = 1, 2, \ldots, n_k \text{ for even numbered bands and} \quad (20)$$

$$\varphi_{kn} = n\, d\varphi_k{}',\ n = 1, 2, \ldots, n_k \text{ for uneven numbered bands.} \quad (21)$$

Each pair (φ_{kn}, θ_k) corresponds to a spatial orientation, assigned to a strut. Ordinal numbers were assigned to each strut of each quarter band of the first octant and of the upper segment. The number of all struts in the Model sample was calculated as a number of the struts in the quarter bands of the first octant multiplied by 8 plus number of struts in the upper segment circular bands multiplied by 2.

The arrays of spherical coordinates φ_i, θ_i corresponding to the quarter bands in the first octant and ring bands on the upper segment were calculated for steps $d\varphi_1 = d\theta = 2.5°$ (36 bands, $N = 816 + 50 = 866$ elements) with a PC code "ANGLES", developed by the author. Transition from quarter bands to circular bands was performed when $\Delta S_{0k} \ge 10\%$ starting from $\theta_k > 0.1964 \approx 11.25°$ (32 quarter bands and four circular bands).

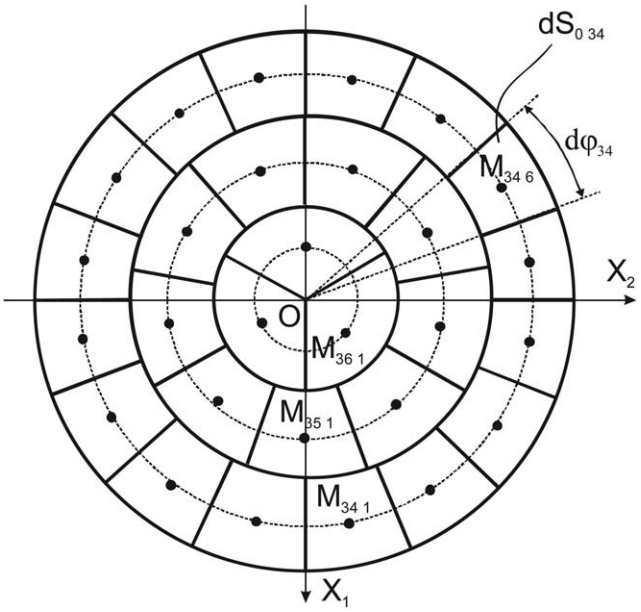

Figure 7. Circular bands number $k = 34$, 35, and 36 of a hemisphere with $n'_k = 16$, 9, and 3 struts.

Three of the four circular bands are depicted in Figure 7. That permitted to retain $\Delta S_{0k} < 5\%$ for all elementary squares. In the result $NN = 8 \times 816 + 2 \times 50 = 6628$ spatial orientations φ_i, θ_i were obtained for the Model sample, Figure 8. The way of the struts' connection into nodes was not considered in the given model.

Struts' Length Distribution in Isotropic Foam

In the result of numerical calculations it was found that the histograms for struts' length samples (Providing length' projections' samples fitting the experimentally determined ones) of mathematical model were asymmetric, with a maximum shifted to the smaller values, i.e. the general character of the struts' length's distribution function was the same as that of the struts' length's projections' distribution function. Therefore the theoretical, numerically calculated struts' length's histograms were smoothed with the probability density function of the following mode:

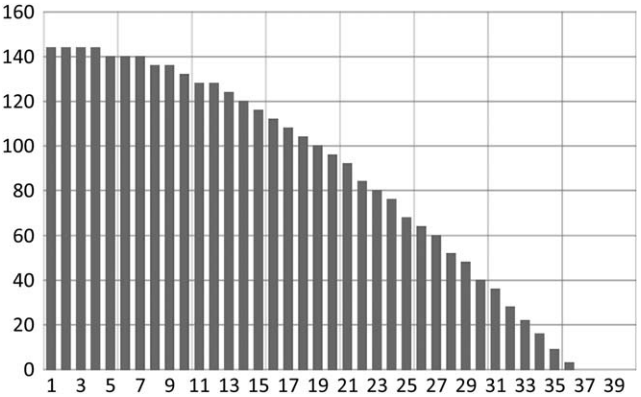

Figure 8. Number of struts in 36 circular bands of a hemisphere; $d\varphi = d\theta = 2.5°$.

Table V. Matrix and the Chain of Elements

Class number i (Value of L_i)	1	2	3	4	5	6	7	8	
Amount of elements	3	4	4	3	2	2	1	1	Chain of elements
n									
1						6			6
2			3						3
3		2							2
4	1								1
5					5				5
6			3						3
7				4					4
8		2							2
9								8	8
10						6			6
11	1								1
12			3						3
13		2							2
14				4					4
15					5				5
16			3						3
17	1								1
18		2							2
19							7		7
20				4					4
Control	3	8	12	12	10	12	7	8	72

$$f(L,q,\alpha,b)=AL^q\exp(-\alpha L^b);\ A=1/\int_{-\infty}^{\infty} f(L,q,\alpha,b)dL. \quad (22)$$

where $q = 1.0$, $b = 1.5$, and $0.02 \leq \alpha \leq 0.35$. The parameter α in isotropic foam was considered to depend solely on foam formulation and other chemical conditions that determine different growth potentials of gaseous bubbles.

The values of 6628 struts′ length in the Model sample were distributed according to function $f(L, \alpha)$, eq. ((22)). A subsample of $N_0 = 100$ struts′ length L subjected to $f(L,\alpha)$ was considered. The length of struts was defined in units, the class width $h = 1$ unit, number of classes I = ROUNDUP(L^{max}) and probability of the i-th class

$$p_i=\Delta p(L_i,\alpha)=f(L_i,\alpha)h,\ L_i \text{ is the biggest value in a class, } i=1,\ 2,\ \ldots,\ I. \quad (23)$$

Frequencies were rounded to the nearest integer value. The subsample was created distributing 100 elements in a matrix [100 $\times$ n^{max}], where n^{max} was the number of the last class, having at least one element. In the result of rounding the final number of elements in several subsamples differed from $N_0 = 100$ slightly ($N_0 = 101$, 99, or 98).

Distribution was performed by a PC code "MATRIX", (*.xls) developed by the author. An example matrix for $n = 20$ demonstrating the distribution principles, is presented in Table V. Each row corresponds to an element of the subsample. Considering parameter $\alpha = 0.16$, the distribution density function was

$$f(L,\alpha)=L\exp(-0.16L^{1.5}) \text{ and } m_i=f(L_i,0.16)n. \quad (24)$$

A control was made at the end of each row and column to avoid empty rows or wrongly filled columns. The last column represents a chain of elements distributed according to the defined probability distribution function.

Struts′ System in Isotropic Foam

The values in the chain were assigned repeatedly to the spatial orientations in the array of 866 orientations. As there is no reason for struts in isotropic foam to be directed predominantly in any direction, the angular distribution was assumed to be even:

$$f_1(\varphi)=\text{const. and } f_2(\theta)=\text{const.} \quad (25)$$

Then the Model sample of 6628 struts with definite length distribution $f = f(L,\alpha)$ and spatially even angular distribution was defined. As a result of symmetry the Model sample was constructed by multiplying the 816 elements in the array of the bands by 8 and 50 elements in the upper segment by 2.

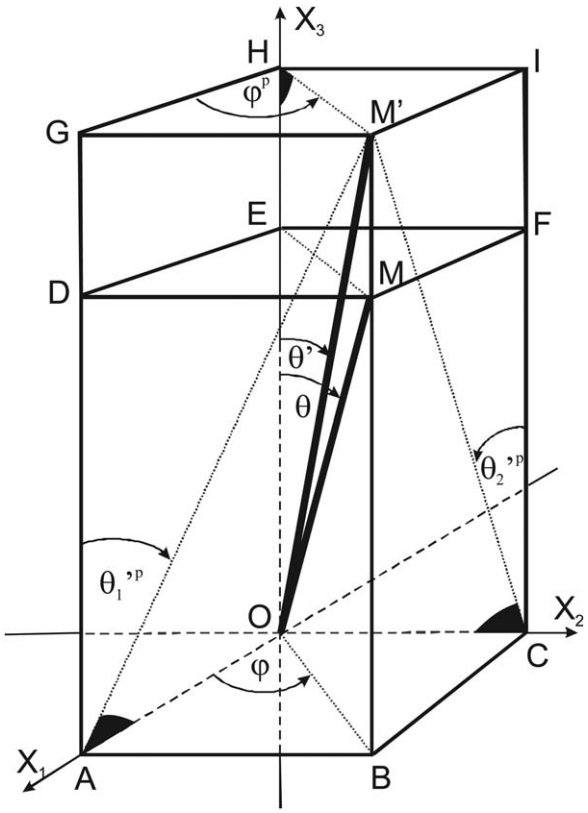

Figure 9. Modelling of a strut and its projections in transtropic foam.

Struts′ System in Transtropic Foam

Coordinates X_1, X_2, and X_3 can be calculated for the end point M of the n-th strut from the Model sample of isotropic foam model, Figure 9:

$$X_{1n}=L_n\sin\theta_n\cos\varphi_n,\ X_{2n}=L_n\sin\theta_n\sin\varphi_n,\ \text{and}\\ X_{3n}=\cos\theta_n,\ n=1,\ 2,\ \ldots,\ \text{NN}. \tag{26}$$

Foam structural anisotropy was implemented by a linear coordinates′ transformation:

$$X_1'=K_1X_1,\ X_2'=K_2X_2,\ X3'=K_3X_3, \tag{27}$$

where K_1, K_2, and K_3 are the coefficients of foam cells elongation degree along axes OX_1, OX_2, and OX_3. Elongation degrees K_1 = 1.0, $K_2 > 1.0$ and $K_3 > 1.0$ for orthotropic foam; $K_1 = K_2 = 1.0$ and $K_3 > 1.0$ for transtropic foam. After transformation $X_3' = K_3 X_3$ the n-th strut′s length L_n = OM became L_n' = OM′:

$$L_n'=L_n\sqrt{\sin^2\theta_n+(K_3\cos\theta_n)^2} \tag{28}$$

and its′ coordinate θ_n became θ_n' = atan $(1/K_3 \tan\theta_n)$; φ_n' = φ_n = const.

Three arrays characterizing 6628 struts of transtropic foam model were calculated: (1) Lengths L_n', (2) Angles θ_n', and (3) Angles φ_n'.

Thus the transtropic foam structural characteristics were derived from the structure of isotropic foam ("Underlying foam").

Projections of Transtropic Foam Struts

Elements on the LM images are projections of the foam strut′s length L' on the image planes X_3 = const.= A, X_2 = const.= B and X_1 = const. = C, Figures 1 and 9. Projections of transtropic foam strut′s length L' on image planes A, B, and C are

$$L_A'P=\text{IM}'=L'\sin\theta',\\ L_B'P=\text{CM}'=[((L'\cos\theta')**2+(L'\sin\theta'\cos\varphi)**2)]^{1/2},\\ L_C'P=\text{AM}'=[((L'\cos\theta')**2+(L'\sin\theta'\sin\varphi)**2)]^{1/2}. \tag{29}$$

Projections of the strut′s angle θ' on planes B and C are

$$\Theta_B'\text{P}=\text{atan}\quad(\tan\theta'\quad\cos\varphi),\\ \Theta_C'\text{P}=\text{atan}\quad(\tan\theta'\quad\sin\varphi) \tag{30}$$

and projection of the angle φ' on plane A is $\varphi'^P = \varphi$ = const. Arrays of (1) length projections $L'^P{}_A$, $L'^P{}_B$, $L'^P{}_C$ and (2) projections of struts′ angles $\Theta'^P{}_C$, $\Theta'^P{}_B$ and φ' were calculated for 6628 struts of transtropic foam model. When K_3 = 1.0, projections of isotropic foam elements were determined. Nodes were considered to be spherical. As projections of a spherical node′s diameter equal to the diameter itself, the diameter can be easily determined from images.

Characterization of Struts′ System from LM Images Data

The transformation [eq. ((27))] does not change the projections of struts′ length on plane A. Experimental investigations[4] have approved that the angular and length distribution of struts′ length projections on plane A remain nearly constant for foam specimens that are cut out from the moulded blocks at different levels even for mould′s dimensions $l_1 \approx l_2$, $l_3 >> l_1, l_2$. At the same time struts′ projections on planes B and C have a more pronounced orientation parallel to RD for specimens cut out from bottom levels in comparison to those cut from top levels.

Therefore it was assumed that for a definite chemical formulation foamed in a open mould with definite l_{31} and l_{32} the distribution of struts′ length′ projections on A comprises information about the underlying struts′ length distribution from which the final transtropic material developed because of the free-rise foaming in a definite mould. The task for characterization of the foam spatial structure comprised: (1) determination of the smoothing functions for experimental struts′ length and angles′ projections on planes A, B, and C, (2) finding such theoretical distribution of struts length in underlying isotropic foam (spatially even distribution) that provides a distribution of struts′ length projections on plane A equal with the experimentally observed one, and (3) finding an elongation degree K_3 that provides such distribution of struts′ lengths and angles that distributions of struts′ length and angles′ projections on planes B and C equal to the experimentally determined ones.

Numerical Calculations

A PC code was developed for numerical calculations, Table VI.

Testing of the model was performed for L = 1.0 and K = 1.0, then $f(X_1{}^P) = f(X_2{}^P) = f(X_3{}^P)$, i.e. a sample of elements of equal length, randomly oriented in the space, had to provide equal

Table VI. Blocks 1 and 2 of the Code "3D FOAM STRUCTURE"

Block 1 "Modelling of isotropic underlying foam"
1 Data input • K = 1.0 isotropic foam • φ and θ of 816 + 50 = 866 spatially evenly distributed struts of subsample • The first approximation for struts' length distribution in underlying isotropic foam: a chain of ≈ 100 struts' length L, distribution $f(L,\alpha_0)$; $\alpha_0 = \alpha^p{}_A{}^E$, where $\alpha^p{}_A{}^E$ is the parameter of smoothing function of experimentally determined struts' length' projections on plane A (Sub code "MATRIX") • Precision ε for smoothing the histograms Go to 3
2 $n = n + 1$ The n-th approximation of underlying isotropic foam struts' length L distribution: a chain of ≈100 struts' length values L, distribution $f(L,\alpha_0)$, where $\alpha_0 = \alpha_A{}^E$ +/- 0.1 × n (Sub code "MATRIX")
3 Formation of a subsample of 866 struts' length L, $f(L,\alpha_0)$ from the chain of ≈100 struts' length
4 Calculation of projections' of struts' length for subsample (866 struts): • $X_1{}^p$, $X_2{}^p$ and $X_3{}^p$ of struts' length L on axis OX_1, OX_2 and OX_3 (Test) • $L^p{}_A$ of struts' length L on planes X_3 = const. = A
5 Formation of Model samples (816 + 2 × 50 = 6628 struts) of struts' length projections': • $X_1{}^p$, $X_2{}^p$ and $X_3{}^p$ • $L^p{}_A$
6 Construction of histograms for Model samples of projections: • $X_1{}^p$, $X_2{}^p$ and $X_3{}^p$ • $L^p{}_A$
7 Smoothing of histograms of Model samples: determination of functions $f(x,\alpha)$ and corresponding parameters α: • $f(X_1{}^p, \alpha_1)$, $f(X_2{}^p, \alpha_2)$, $f(X_3{}^p, \alpha_3)$, and α_1, α_2, α_3 • $f(L^p{}_A, \alpha_A)$ and α_A
8 Testing of model: If L = 1.0 and K = 1.0 (Isotropic foam), then $f(X_1{}^p) = f(X_2{}^p) = f(X_3{}^p) \neq f(\alpha)$
9 Comparison of theoretical distribution function $f(L^p{}_A,\alpha^p{}_A)$ with function $f^E(L^p{}_A, \alpha^p{}_A{}^E)$, smoothing the histograms, determined experimentally from images A (Sub code "FUNCTIONS"): • Good correspondence: go to 10 • Bad correspondence: go to 2
10 Underlying isotropic foam have struts' length distribution $f(L, \alpha_0)$, α_0
11 End
Block 2 "Modelling of transtropic foam"
1 Data input • φ and θ of spatially evenly distributed struts of subsample (816 + 50 = 866 struts) • Underlying isotropic foam strut length' distribution $f(L, \alpha_0)$ (866 struts) • The 1-st approximation of transtropic foam cells elongation degree $K^E{}_3 = d^{pE}{}_{3aver}/d^{pE}{}_{1aver} = d^{pE}{}_{3aver}/d^{pE}{}_{2aver}$; where $d^{pE}{}_{1aver}$, $d^{pE}{}_{2aver}$ and $d^{pE}{}_{3aver}$ are cell's diameters' average projections, determined experimentally from images A, B, and C • Precision ε for smoothing the histograms Go to 3
2 $n = n + 1$ The n-th approximation of elongation degree: $K_3 = K_3{}^E \pm 0.1 \times n$
3 Implementation of transtropy into subsamples (866 elements) of isotropic foam struts' length and angles: $X_1' = X_1$, $X_2' = X_2$ and $X_3' = K_3 X_3$ $\Theta' = a\tan(1/K_3 \tan\theta)$; $\varphi' = \varphi$ = const.
4 Formation of Model samples (816 + 2 × 50 = 6628 struts) of struts' length L' and angles Θ'

TABLE VI. *Continued*

5	Calculation of struts' length and angles' projections' for subsample (866 struts): • L'^{p}_{B} and L'^{p}_{C} • Θ'^{p}_{B} and θ'^{p}_{C}
6	Formation of Model samples (6628 struts) of struts' length and angles' projections' • L'^{p}_{B} and L'^{p}_{C} • Θ'^{p}_{B} and θ'^{p}_{C}
7	Construction of histograms for Model samples (6628 struts) of projections of struts' length and angles': • L'^{p}_{B} and L'^{p}_{C} • Θ'^{p}_{B} and θ'^{p}_{C}
8	Smoothing histograms of struts' length and angles' projections' Model samples: determination of distribution functions f, h and corresponding parameters α, β: • $f(L'^{p}_{B}, \alpha^{p}_{B})$ and $f(L'^{p}_{C}, \alpha^{p}_{C})$; α^{p}_{B} and α^{p}_{C} • $h(\theta'^{p}_{B}, \beta^{p}_{B})$ and $h(\theta'^{p}_{C}, \beta^{p}_{C})$; β^{p}_{B} and β^{p}_{C}
9	Comparison of theoretical distribution functions $f(L^{p}_{B}, \alpha^{p}_{B})$ and $f(L^{p}_{C}, \alpha^{p}_{C})$ and $h(\theta'^{p}_{C}, \beta^{p}_{C})$, $h(\theta'^{p}_{B}, \beta^{p}_{B})$ with functions $f^{E}(L^{p}_{B}, \alpha^{p}{}_{B}{}^{E})$ and $f^{E}(L^{p}_{C}, \alpha^{p}{}_{C}{}^{E})$ and $h^{E}(\theta'^{p}_{C}, \beta^{p}_{C})$, $h^{E}(\theta'^{p}_{B}, \beta^{p}_{B})$ smoothing the histograms, determined experimentally from images B and C (Sub code "FUNCTIONS"): • Good correspondence: go to 10 • Bad correspondence: go to 2
10	Constructing histograms for Model samples of struts' length L' and angles θ'
11	Smoothing histograms of struts' length L' Model sample: determination of functions $f(L', \alpha_4)$ and corresponding parameters α_4
12	Transtropic foam have struts' length distribution $f(L', \alpha_4)$ and angles' θ' distribution histograms $p(\theta')$
13	End

samples of projections $X_1{}^{p}$, $X_2{}^{p}$, and $X_3{}^{p}$ on the coordinate axis X_1, X_2, and X_3:

$$X_1^p = L' \sin\theta \cos\varphi';\ X_2^p = L' \sin\theta \sin\varphi';\ \text{and}\ X_3^p = L' \cos\theta. \quad (31)$$

Testing provided approving results. The Model sample of 6628 struts' length L' having length probability density distribution $f = f(L', \alpha_4)$ and spatially uneven angular distribution was calculated. The parameters $\alpha^{p}{}_{A}{}^{E}$, $\alpha^{p}{}_{B}{}^{E}$, and $\alpha^{p}{}_{C}{}^{E}$ were determined using LM images, Table III. As the transformation [eq. ((27))] does not change the strut's length projections in the plane X_3 = const. = A, arrays of projections of the struts' length on A have to be equal for isotropic and anisotropic foam, i.e. not dependent on elongation degree K_3. The parameter value $\alpha_0 = \alpha^{p}{}_{A}{}^{E}$ was entered as the first approximation, where $\alpha^{p}{}_{A}{}^{E}$ was parameter of theoretical distribution function of experimentally determined struts' length' projections on image plane A.

The arrays of length' projections $L'^{p}{}_{A}$, $L'^{p}{}_{B}$, and $L'^{p}{}_{C}$ were calculated and histograms were constructed. Theoretical distribution functions were found for the histograms. The functions were compared with the ones for experimentally determined histograms and the next approximation for α_A was defined. As a rule 2–3 iterations were enough to find the best fitting value of α_0 for underlying foam struts' length probability density function $f(L,\alpha_0)$.

Practically, instead of a straight-away iteration process for determination of K_3, it was convenient to perform calculations for fixed values of K_3 first: K_3 = 1.0, 1.5, 2.0, 2.5, and 3.0. The K_3 value providing the closest fit to the experimental data was used as input value for the first iteration and precise determination of K_3.

RESULTS AND DISCUSSION

Special Cases

At first numerical calculations for several special cases of the mathematical model were performed, class width h = 1.0. Case 1: elongation degree varied. All initially spatially and evenly distributed struts (Underlying foam) have equal initial length L = 10.0 units = const., $f(1.0)$ = 1.0 and elongation degree varies $1.0 \le K_3 \le 3.0$. The graph of probability density distributions $f(L'^{p}{}_{A}) = f(L'^{p}{}_{B}) = f(L'^{p}{}_{C})$ for projections' $L'^{p}{}_{A}$, $L'^{p}{}_{B}$, and $L'^{p}{}_{C}$ samples when K_3 = 1.0 are presented in Figure 10.

Graphs of probability density distribution f for projections $L'^{p}{}_{A}$, $L'^{p}{}_{B}$, and $L'^{p}{}_{C}$ when K_3 = 2.0 are presented in Figure 11. Graphs of f for $L'^{p}{}_{B}$ and $L'^{p}{}_{C}$ when K_3 equals: (a) 1.0, (b) 1.1, (c) 1.3, (d) 1.5, (e) 2.0, and (f) 3.0 are presented in Figure 12. When K_3 = 1.0, $f(L'^{p}{}_{A}) = f(L'^{p}{}_{B}) = f(L'^{p}{}_{C})$. It is important to note that graphs of distribution $f(L'^{p}{}_{A})$ retain the same character for any value of K_3 and graphs of distributions $f(L'^{p}{}_{B})$ and $f(L'^{p}{}_{C})$ are equal: $f(L'^{p}{}_{B}) \approx f(L'^{p}{}_{C})$ because of transtropy.

Cases 2–7: Underlying isotropic foam varied. All struts are distributed spatially evenly: K_3 = 1.0 = const., but have different initial length 1.0 unit $\le L \le$ 15.0 units. If K_3 = 1.0, there is no elongation and $L' = L$. Function $f(L')$ is: (a) Even $f(L)$ = 1/15 = 0.067 (Figure 13), (b) Increasing (Figure 14), (c) Decreasing (Figure 15), (d) Symmetrically triangular (Figure 16), (e) Normal (Figure 17), and (f) Asymmetric according to eq. ((22)) (Figure 18). In isotropic foam the mode (As maximum) of distribution of struts' projections shifts for several units to the

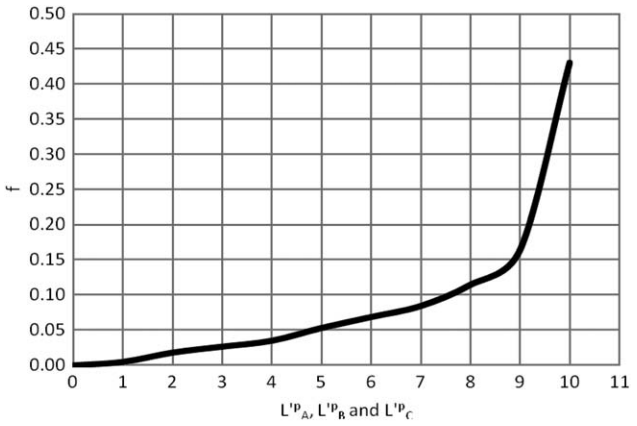

Figure 10. Distribution f of L'^{p}_{A}, L'^{p}_{B}, and L'^{p}_{C} for L = 10 units = const. and K_3 = 1.0.

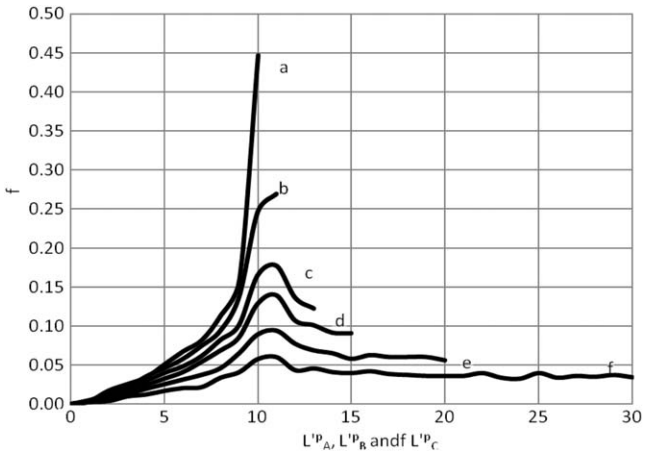

Figure 12. Distribution f of L'^{p}_{B} and L'^{p}_{C} for L = 10.0 units = const. and K_3 values (a) 1.0, (b) 1.1, (c) 1.3, (d) 1.5, (e) 2.0, and (f) 3.0.

smaller values compared to mode of distribution of struts themselves. (Figures 16–18).

The results obtained for even, increasing, decreasing, and symmetrically triangular distribution functions are similar to those reported in classical investigations[5,6] for modelling distribution functions of bubbles′ radii from distribution of circles′ radii on the low-porosity foam sample′s cross section ($\rho_f \approx 220$ kgm^{-3}). At the same time the numerical values of f for projections of a single element value (strt length or sphere′s diameter) differ as the functions of projections are different.

Struts′ Length

The numerical calculation results revealed: when elongation degree of foam structure $K_3 \geq 3.0$, distribution of struts′ length projections on planes B and C is nearly equal to distribution of struts′ length L': $\alpha_B \approx \alpha_C \approx \alpha_4$ and $f(L'^{p}_{B}) \approx f(L'^{p}_{C}) \approx f(L')$. For several experimental specimens $f(L'^{p}_{B}) \approx f(L'^{p}_{C}) \approx f(L')$ was achieved already at K_3 = 2.5. The struts are oriented along axis O3 to such a degree that statistical samples of their projections on planes B and C differ little from the samples of struts′ length themselves. It means, when foam are markedly transtropic, struts′ length characteristics can be determined with a sufficient precision from image B (or C) alone, without analysis of image A. Further K_3 was varied in a range $1.0 \leq K_3 \leq 3.0$ for each underlying foam (α_0).

The calculated parameters α_B and α_C were compared with the experimental values, Table III, the fitting ones and the corresponding K_3 were determined, Table VII. For all experimental specimens from cubes 1 parameter α_0 of the underlying foam was bigger (dispersion of L values was smaller) than for foam from the cubes 2. Different foaming conditions at different heights of a foam block could exist, e.g. a higher pressure at the bottom of the block could prevent dispersion in bubbles′ radii and lead to a smaller dispersion of the struts′ length.

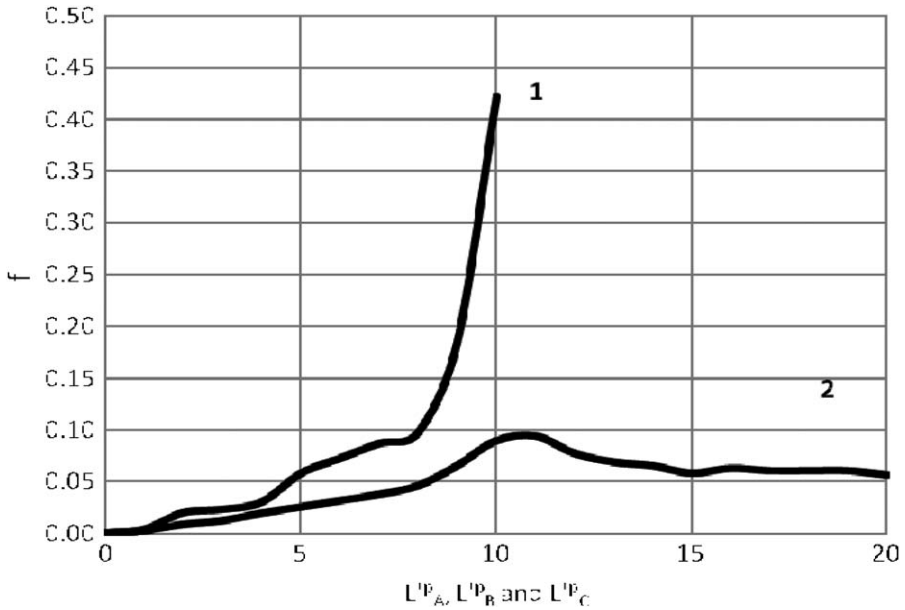

Figure 11. Distribution f of 1) L'^{p}_{A} and 2) L'^{p}_{B} and L'^{p}_{C} for L = 10 units = const. and K_3 = 2.0.

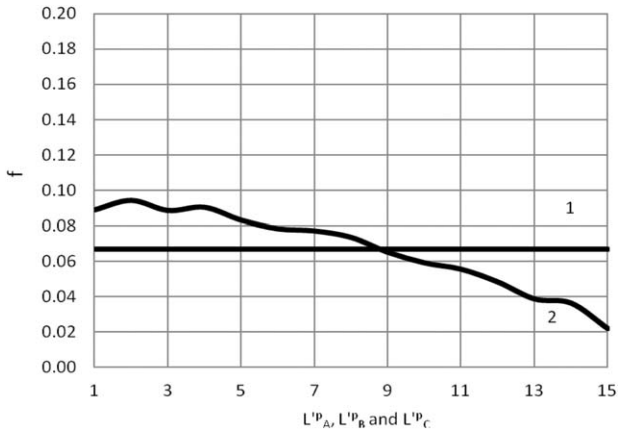

Figure 13. (1) $f(L)$ and (2) $f(L^P_A)$, $fp(L^P_B)$ and $f(L^P_C)$; $K_3 = 1.0$.

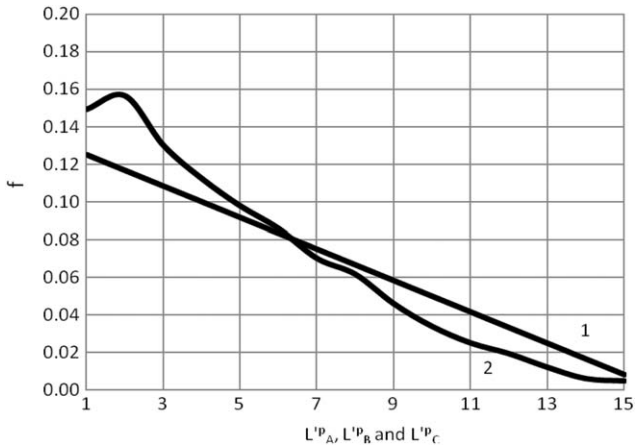

Figure 15. (1) $f(L)$ and (2) $f(L^P_A)$, $f(L^P_B)$, and $f(L^P_C)$; $K_3 = 1.0$.

Figure 19 presents dependence of parameter α_4 of struts′ length distribution $f(L',\alpha_4)$ on elongation degree K_3 for different underlying foam: (1) $\alpha_0 = 0.06$, (2) $\alpha_0 = 0.12$, and (3) $\alpha_0 = 0.25$ (the smallest, the medium and the biggest values). The smaller is the parameter α_0, the more dispersed are the values of struts′ length in the sample. Figure 20 presents α_4 of $f(L',\alpha_4)$ in dependence of underlying foam parameter α_0 for different elongation degrees: (1) $K_3 = 1.0$, (2) $K_3 = 2.0$, and (3) $K_3 = 3.0$.

To find the modal class of a variable x distributed according to $f(x)$, the value x_M corresponding to the maximum of $f(x) = x\exp(-\alpha x^{1.5})$ was determined from the condition of extreme:

$$f'(x)=\exp(-\alpha x^{1.5})(1-1.5\alpha x^{1.5})=0,\ \text{then}\ x_M=0.763\,\alpha^{2/3}, \quad (32)$$

where $x_M = L'_M$, L'^P_{BM}, or L'^P_{CM}. Dependence of x_M on α was presented in Figure 21.

Calculation results for probability distributions of struts′ length $f(L', \alpha_4)$ and struts′ length projections′ $f(L'^P, \alpha^P_B)$ of foam specimens were presented in Tables VIII and IX. Several sources[8,19] report $N = 200$ elements in a statistical sample as the smallest amount sufficient for determination of distribution functions. For practical purposes it would be necessary to know L'^{200}_{max}: value of the biggest strut length in a sample of 200 struts. E.g., if length measurements of 200 struts from the experimental specimen 1-2 would be available there would be one, the longest strut having length $L'^{200}_{max} = 26$ units = 0.47 mm.

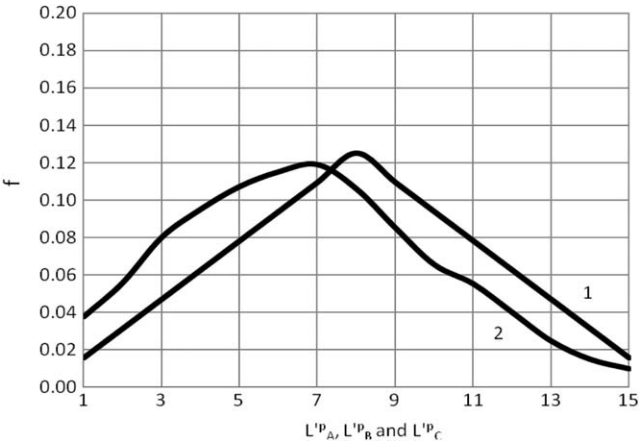

Figure 16. (1) $f(L)$ and (2) $f(L^P_A)$, $f(L^P_B)$, and $f(L^P_C)$; $K_3 = 1.0$.

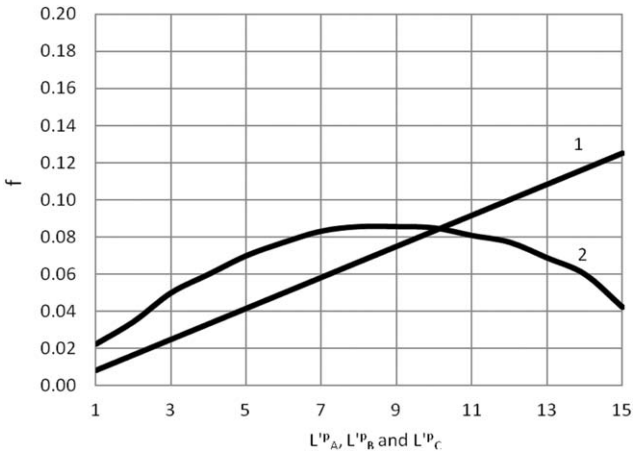

Figure 14. (1) $f(L)$ and (2) $f(L^P_A)$, $f(L^P_B)$, and $f(L^P_C)$; $K_3 = 1.0$.

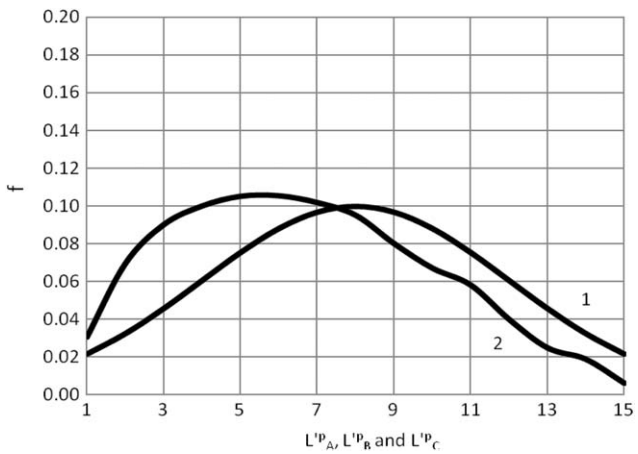

Figure 17. (1) $f(L)$ and (2) $f(L^P_A)$, $f(L^P_B)$, and $f(L^P_C)$; $K_3 = 1.0$.

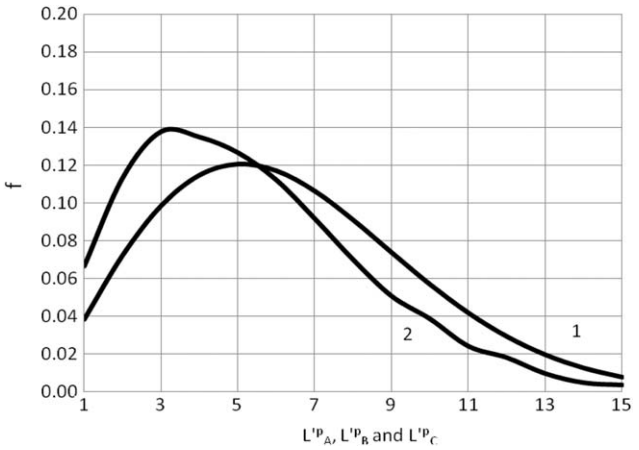

Figure 18. (1) $f(L)$ and (2) $f(L^P{}_A)$, $f(L^P{}_B)$, and $f(L^P{}_C)$; $K_3 = 1.0$.

Probability densities of struts length $f(L')$ and $f(L'^P{}_B)$ of struts' length projections on plane B (or on plane C) for specimens 2-2 and 4-2 were presented in Figure 22. Because of the small values of elongation degree $K_3 = 1.2$ and $K_3 = 1.1$ these specimens revealed the biggest differences between $f(L')$ and $f(L'^P{}_B)$. The general character of struts' length distribution functions corresponds well to the one determined for cells' average diameters by the method of mercury absorption tests in Ref. 1.

Struts' length L' probability density functions $f(L')$ for specimens from the second cube 1-2, 2-2, …, 5-2 were presented in Figure 23 (Scale 1 unit = 1/55 mm applied). In general specimens from the cubes number 2 revealed bigger differences between $f(L')$ and $f(L'^P{}_B)$ than specimens from cubes number 1. That corresponds to experimental data[4]: foam at the bottom of the mould have more extended cells than at the top.

For practical purposes it would be necessary to know the relative difference R between the struts' average projection on planes B (C) and average strut length: $R = (L'^P{}_{B\text{aver}} - L'_{\text{aver}})/L'^P{}_{B\text{aver}}$. Calculations showed that value of R is the biggest for isotropic foam $K_3 = 1.0$: R ≈ 30%. When elongation degree increases to $K_3 = 3.0$, R reduces to $R \approx 10\%$, Figure 24. The dependence $R = R(K_3)$ can be approximated by a function

$$R(K_3) = R_0\, K_3^{1.05}, \text{ where } R_0 = R(K_3 = 1.0) = 28\%. \tag{33}$$

For the majority of industrially manufactured PUR foam cells elongation degree is not high $K_3 \leq 1.30$,[1–3] as isotropy of mechanical properties is mostly required in practical applications and difference $28\% \leq R \leq 24\%$.

Struts' Angles

Modelling and numerical calculations' results showed that distribution of struts' angles φ as well as projections φ^p on plane A was even:

$$f(\varphi) = f(\varphi^p_A) = 1/(2\pi), \text{ as } \varphi = \varphi^p_A. \tag{34}$$

Even distribution was retained after implementation of transtropy [eq. ((27))], too:

$$\varphi' = \varphi = \text{const. and } f(\varphi'^p_A) = f(\varphi^p_A). \tag{35}$$

Measurements of projections $\varphi'^P{}_A$ from LM images A approved the even character of angles φ' and $\varphi'^P{}_A$ distribution for foam blocks 1–5, considered.

Distribution of angles θ' of the struts in Model sample at: (a) $K_3 = 1.0$; isotropic foam and (b) $K_3 = 3.0$; anisotropic foam was presented on Figure 25, class width $\Delta\theta' = 10°$. Here and further the first octant was considered. The histograms of angles and their projections were the same for other octants, too for isotropic and transtropic foam: $p(\theta') = p(180 - \theta')$, $\theta' \leq 90°$. Figure 25 shows a characteristic feature of the mathematical model when $K_3 = 1.0$ (isotropic structure): although the projections θ'^P of $\theta = \theta'$ are distributed evenly on an image plane, the angles $\theta = \theta'$ have an uneven distribution with regard to axis OX_3 of a Cartesian reference system, arbitrary placed in the space. At the same time angular distribution of struts is even with regard to an arbitrary spatial angle $d\omega$. A certain roughness of the trend in histogram at $K_3 = 3.0$ exists because of finite value of division steps $d\varphi_1 = d\theta = 2.5°$.

Values of projections θ'^P of angle's θ' in the Model sample were calculated and sorted into nine classes, class width $\Delta\theta'^P = 10°$. The distribution of projections $\theta'^P{}_B$ (or $\theta'^P{}_C$) on planes B (or C) was even for the Model sample of struts $f(\theta'^P{}_B) = 1/9$ when $K_3 = 1.0$, Figure 26. When $K_3 = 3.0$ the relative amount of smaller projections $\theta'^P{}_B$ (or $\theta'^P{}_C$) increased in comparison to case when $K_3 = 1.0$.

The calculation results were compared with experimental data for the specimens 4-2 and 1-1. Specimen 4-2 had the lowest elongation degree among the specimens, considered: $K_3 = 1.08 \approx 1.1$ and its structure was the most close to isotropic foam structure. The experimental data histogram was built for a statistical sample of 300 elements $\theta'^P{}_{BC}$, 150 measured from LM image B and 150 from image C, Figure 27.

The distribution of angle's θ' projections θ'^P was further considered for the experimental specimen 1-1 that had the highest elongation degree $K_3 = 2.50$ among the specimens, considered. The experimental histogram was built for a statistical sample of 300 elements $\theta'^P{}_{BC}$, 150 determined from LM image B and 150 from image C, Figure 28.

A good correspondence of experimental data with modelling results was observed. The differences could be explained by the existence of some close order of gas bubbles in the foaming composition as well as action of Earth gravitation on the soft polymer in the struts of foaming composition that were not taken into account in the mathematical model.

The general character of experimental and modelling data histograms for angle's θ' projections $\theta'^P{}_B$ and $\theta'^P{}_C$ (Figures 26–28) suggested choosing the smoothing function of an exponential mode:

$$h(\theta', \beta) = A \exp\left[-(\theta'/10)^{\beta}\right],\ \theta' > 0,\ \beta > 0,$$
$$h(\theta',\ \beta) \geq 0 \text{ and } A = 1/\int_0^{90} h(\theta', \beta)\, d\theta', \tag{36}$$

where β is a parameter. For the experimental specimens considered $0.13 \leq \beta \leq 0.50$. The best fitting for the most anisotropic

Table VII. Results: „M" – Calculations, „E" – Experiments, „IS" – Isotropic, and „TR" – Transtropic

N	Specimen	Data correspondence	$\alpha^{p}{}_{A}{}^{E}$	α_0	K_3	$\alpha^{p}{}_{B}$	$\alpha^{p}{}_{C}$	α_4	Aniso-tropy mode	*R* (%)
1	1-1	M	0.15	0.12	1.0	0.15	0.15	0.12	IS	28
2		M			1.1	0.13	0.13	0.10	TR	26
3		M			1.5	0.10	0.10	0.09	TR	19
4		M			2.0	0.09	0.09	0.08	TR	14
5		**M, E**			**2.5**	**0.06**	**0.06**	**0.06**	**TR**	**11**
6		M			3.0	0.05	0.05	0.05	TR	8
1	1-2	M	0.12	0.09	1.0	0.12	0.12	0.09	IS	28
2		M			1.1	0.09	0.09	0.08	TR	26
3		M			1.5	0.08	0.08	0.06	TR	19
4		M			2.0	0.06	0.06	0.05	TR	14
5		**M, E**			**2.5**	**0.05**	**0.05**	**0.04**	**TR**	**11**
1	2-1	M	0.13	0.10	1.0	0.13	0.13	0.10	IS	28
2		M			1.1	0.13	0.13	0.10	TR	26
3		**M, E**			**1.5**	**0.09**	**0.09**	**0.08**	**TR**	**19**
4		M			2.0	0.08	0.08	0.06	TR	14
5		M			2.5	0.06	0.06	0.05	TR	11
1	2-2	M	0.089	0.06	1.0	0.09	0.09	0.06	IS	28
2		M			1.1	0.08	0.08	0.05	TR	26
3		**M, E**			**1.2**	**0.075**	**0.075**	**0.05**	**TR**	**25**
4		M			1.5	0.06	0.06	0.04	TR	19
5		M			2.0	0.04	0.04	0.04	TR	14
6		M			2.5	0.04	0.04	0.03	TR	11
7		M			3.0	0.03	0.03	0.03	TR	8
1	3-1	M	0.31	0.25	1.0	0.31	0.31	0.25	IS	28
2		M			1.1	0.25	0.25	0.20	TR	26
3		M			1.5	0.22	0.22	0.18	TR	19
4		**M, E**			**2.0**	**0.16**	**0.16**	**0.14**	**TR**	**14**
5		M			2.5	0.13	0.13	0.13	TR	11
6		M			3.0	0.12	0.12	0.10	TR	8
1	3-2	M	0.23	0.20	1.0	0.23	0.23	0.20	IS	28
2		M			1.1	0.20	0.20	0.17	TR	26
3		M			1.5	0.18	0.18	0.13	TR	19
4		**M, E**			**2.0**	**0.13**	**0.13**	**0.12**	**TR**	**14**
5		M			2.5	0.10	0.10	0.10	TR	11
1	4-1	M	0.31	0.25	1.0	0.31	0.31	0.25	IS	28
2		M			1.1	0.25	0.25	0.20	TR	26
3		**M, E**			**1.5**	**0.22**	**0.22**	**0.16**	**TR**	**19**
4		M			2.0	0.16	0.16	0.14	TR	14
5		M			2.5	0.13	0.13	0.13	TS	11
6		M			3.0	0.12	0.12	0.10	TR	8
1	4-2	M	0.27	0.23	1.0	0.27	0.27	0.23	IS	28
2		**M, E**			**1.1**	**0.25**	**0.25**	**0.18**	**TR**	**26**
3		M			1.3	0.22	0.22	0.16	TR	22
4		M			1.5	0.22	0.22	0.15	TR	19
5		M			2.0	0.16	0.16	0.13	TR	14
6		M			2.5	0.13	0.13	0.12	TR	11
1	5-1	M	0.29	0.23	1.0	0.29	0.29	0.23	IS	28

TABLE VII. *Continued*

N	Specimen	Data correspondence	$\alpha^p{}_A{}^E$	α_0	K_3	$\alpha^p{}_B$	$\alpha^p{}_C$	α_4	Aniso-tropy mode	R (%)
2		M			1.1	0.26	0.26	0.18	TR	26
3		M			1.5	0.22	0.22	0.15	TR	19
4		**M, E**			**1.7**	**0.18**	**0.18**	**0.14**	**TR**	**17**
5		M			2.0	0.16	0.16	0.13	TR	14
6		M			2.5	0.13	0.13	0.12	TR	11
1	5-2	M	0.29	0.23	1.0	0.29	0.29	0.23	IS	28
2		M			1.1	0.26	0.26	0.18	TR	26
3		M			1.5	0.22	0.22	0.15	TR	19
4		**M, E**			**1.6**	**0.20**	**0.20**	**0.15**	**TR**	**18**
5		M			2.0	0.16	0.16	0.13	TR	14
6		M			2.5	0.13	0.13	0.12	TR	11

specimen 1-1, $K_3 = 2.5$ was at $\beta = 0.50$, for the most isotropic one 4-2, $K_3 = 1.1$ at $\beta = 0.13$. For isotropic foam, $K_3 = 1.0$ parameter $\beta \approx 0.02$ and probability $p(\theta'^p{}_B) = 1/9 = 0.11 =$ const. The fitting of theoretical data to the exponential smoothing function was very good: $\lambda \leq 0.3$ and $p(\lambda) \approx 1.0$ and average of the experimental data: $\lambda \leq 0.8$ and $p(\lambda) \approx 0.54$ (Kolmogorov's criterion).[19]

An orientational parameter g is often used to characterize cumulatively the angular orientation of elements in a statistical sample (e.g. short glass fibers in a polymer matrix)[8]:

$$g = 2 < \cos^2\theta > -1; \text{ where } < \cos^2\theta > = \frac{\sum n(\theta)\cos^2\theta}{\sum n(\theta)}, \quad (37)$$

$n(\theta)$ is the number of length elements having spherical angle θ. The values of $g = \pm 1$ indicate two completely aligned states along the directions $\theta = 0°$ and 90°. When $g = 0$ the orientations of elements are considered to be completely random in Ref. 8. To compare two model assumptions, the g values were

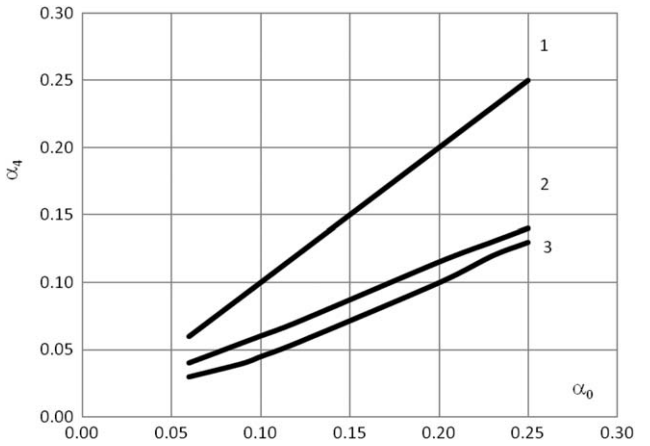

Figure 20. The parameter α_4 of $f(L, \alpha_4)$ in dependence of α_0 for K_3 values (1) 1.0, (2) 2.0, and (3) 3.0.

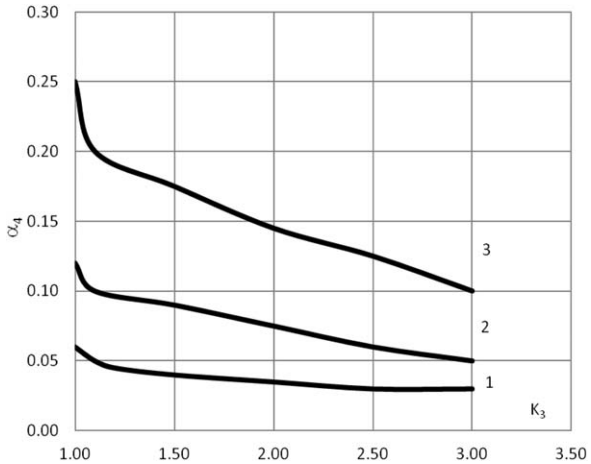

Figure 19. The parameter α_4 of $f(L,\alpha_4)$ in dependence of K_3 for α_0 values (1) 0.06, (2) 0.12, and (3) 0.25.

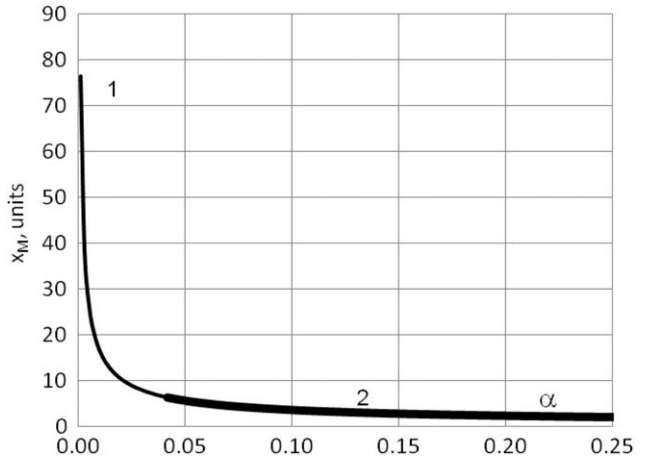

Figure 21. Dependence of x_M on α for (1) $0.001 \leq \alpha \leq 0.25$ and (2) specimens 1-1,…, 5-2; $0.042 \leq \alpha \leq 0.25$.

Table VIII. Characteristics of Struts' length L' Probability Distribution; Calculation Results

Specimen	α_4	L'_{aver} (units)	L'_{mod} (units)	$f(L'_{mod})$	Modal class Nr	$L'_{max}{}^{200}$ (units)	s (units)	v (%)
1-1	0.06	7.4	5.1	0.106	6	21	4.9	66
1-2	0.04	8.9	6.4	0.079	7	26	5.8	57
2-1	0.08	6.1	4.0	0.119	5	18	3.5	58
2-2	0.05	7.5	5.5	0.092	6	22	4.2	56
3-1	0.14	4.0	2.8	0.179	3	12	2.4	61
3-2	0.12	4.7	3.2	0.159	4	14	2.8	60
4-1	0.16	3.4	2.6	0.196	3	11	1.9	57
4-2	0.18	3.1	2.4	0.209	3	11	1.7	55
5-1	0.14	3.7	2.8	0.179	3	12	2.1	58
5-2	0.15	3.6	2.7	0.185	3	12	2.1	57

calculated, Table X for the samples of angles θ' for the (1) proposed model of spatially random distribution of struts: dS_0 = const. ($d\varphi \neq d\theta$) and for (2) distribution model determined by equality of the steps over spherical angles $d\varphi = d\theta$ = const. ($dS_0 \neq$ const.). When dS_0 = const., values of g were calculated also for samples of (1.1) θ' at $\varphi' = 45°$ and (1.2) $\theta'^{p}{}_{B}$ (or $\theta'^{p}{}_{C}$).

Several numerical tests of model based on assumption $d\varphi = d\theta$ were performed at $K_3 = 1.0$ (isotropic foam, random spatial distribution of struts in actual material). The samples of strut length projections $L^{p}{}_{A}$, $L^{p}{}_{B}$, and $L^{p}{}_{C}$ were calculated and found to be considerably different as well as distributions of angles θ' projections $\theta'^{p}{}_{B}$ and $\theta'^{p}{}_{C}$ were found to be not even. Since that does not correspond with experimental data, the model was rejected. Both tests provided results corresponding with experimental data for assumption dS_0 = const.

Comparison with Experimental Data

To perform additional comparison of modelling results, Table VII with the available experiment data, Table III, the following method was used. Data of Table III were divided in two groups of experimental specimens: (1) 1-1, …, 2-2 having $0.09 \leq \alpha^{p}{}_{A}{}^{E} \leq 0.15$ and (2) 3-1, …, 5-2 having $0.23 \leq \alpha^{p}{}_{A}{}^{E} \leq 0.31$. Average value of $\alpha^{p}{}_{A}{}^{E}$ for both groups was calculated: (1) $\alpha^{p}{}_{A}{}^{Eaver} \approx 0.12$ and (2) $\alpha p_{A}{}^{Eaver} \approx 0.28$. The averaged parameter $\alpha^{p}{}_{A}$ of struts' projections' distribution in plane A $\alpha^{p}{}_{A}{}^{aver}$ was assigned to all specimens in a group. Since a definite α_0 of underlying isotropic foam corresponds to each $\alpha^{p}{}_{A}{}^{E}$, the corresponding α_0 was calculated. Thus an equal underlying struts' length distribution $f(\alpha_0)$ was provided for all specimens in a group: (1) $\alpha_0 = 0.09$ and (2) $\alpha_0 = 0.23$.

Among the theoretical data sets the best fitting experimental specimens with regard to the averaged $\alpha^{p}{}_{A}{}^{Eaver}$ are (1) 1-2 in the first group and (2) 5-1 in the second one, Table VII. Theoretical graphs of struts' length projections' on plane B (or C) distribution parameter $\alpha^{p}{}_{B} = \alpha^{p}{}_{B}(K_3)$ for 1-2 and 5-1 were depicted in Figure 29 for elongation degrees $1.0 \leq K_3 \leq 3$ together with experimental data of other specimens from groups 1 and 2. A good correspondence was found to exist between the theoretical and experimental data, therefore it was concluded that the proposed model adequately described the main characteristics of isotropic and transtropic free-rise foam strut-like structure.

CONCLUSIONS

In the given investigation the following main results were obtained:

1. A methodology was developed for preparing transtropic foam experimental specimens and investigation of open-cell

Table IX. Characteristics of Struts' Length Projections' $L'^{p}{}_{B}$ (or $L'^{p}{}_{C}$) Probability Distribution, Calculation Results

Specimen	$\alpha^{p}{}_{B}$	$L'^{p}{}_{Baver}$ (units)	$L'^{p}{}_{Bmod}$ (units)	$f(L'^{p}{}_{Bmod})$	Modal class Nr	$L'^{p}{}_{Bmax}{}^{200}$ (units)	s (unit)	v (%)
1-1	0.06	6.6	5.1	0.106	6	20	4.9	74
1-2	0.05	8.0	5.9	0.092	6	22	5.9	73
2-1	0.09	5.2	3.8	0.132	4	16	3.4	66
2-2	0.07	6.2	4.3	0.119	5	18	4.0	65
3-1	0.16	3.5	2.6	0.196	3	11	2.4	70
3-2	0.13	4.1	2.9	0.173	3	13	2.8	68
4-1	0.22	2.8	2.1	0.241	3	9	1.9	66
4-2	0.25	2.4	1.9	0.269	2	9	1.5	63
5-1	0.18	3.2	2.4	0.196	3	11	2.1	67
5-2	0.20	3.0	2.2	0.209	3	11	2.0	66

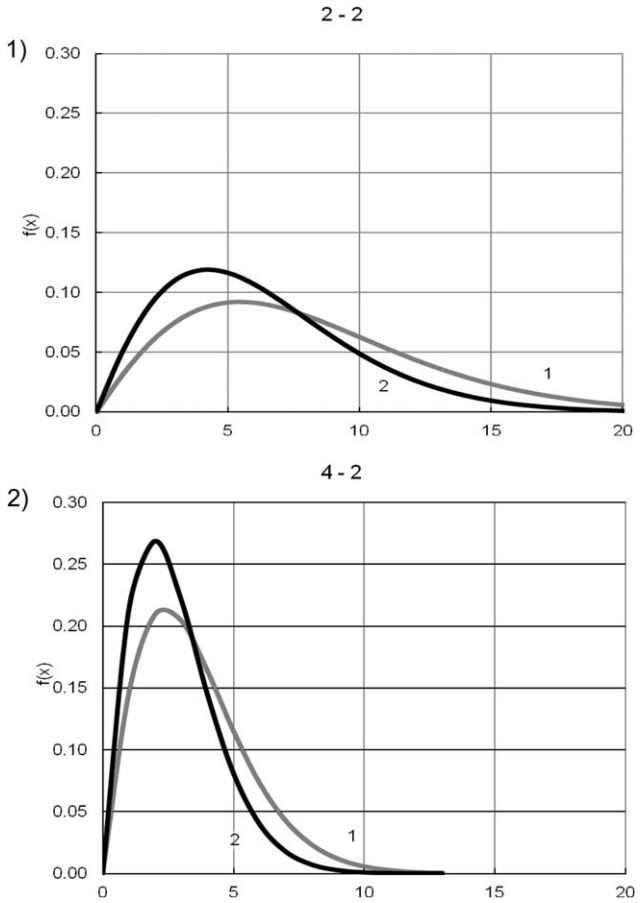

Figure 22. Probability distribution (1) $f(L')$ and (2) $f(L'^{p}_{B})$ for specimens 2-2 and 4-2.

highly porous plastic foam structure with LM by taking images in three mutually perpendicular planes corresponding to the principal symmetry axis of foam. Projections of the main load-carrying elements—polymeric struts′ length and angles on planes A, B, and C were determined for 10 transtropic foam experimental specimens, ρ_f = 33, …, 79 kg m^{-3} for statistical samples of up to 300 elements. Parameters of the theoretical distribution functions smoothing the experimentally determined histograms of struts′ projections were calculated.

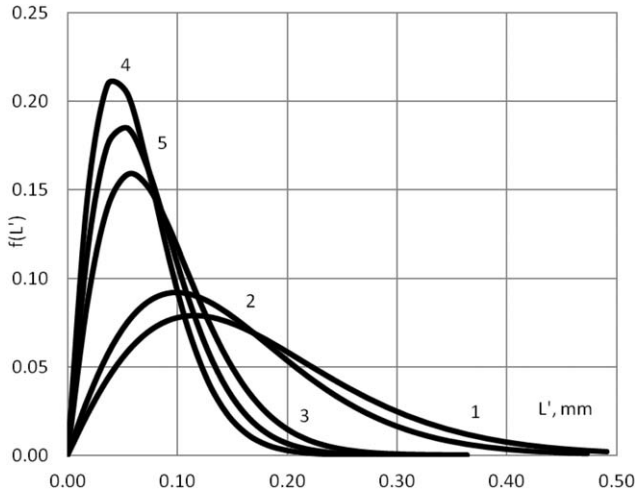

Figure 23. Struts' length distribution $f(L')$ for specimens (1) 1-2, (2) 2-2, (3) 3-2, (4) 4-2, and (5) 5-2.

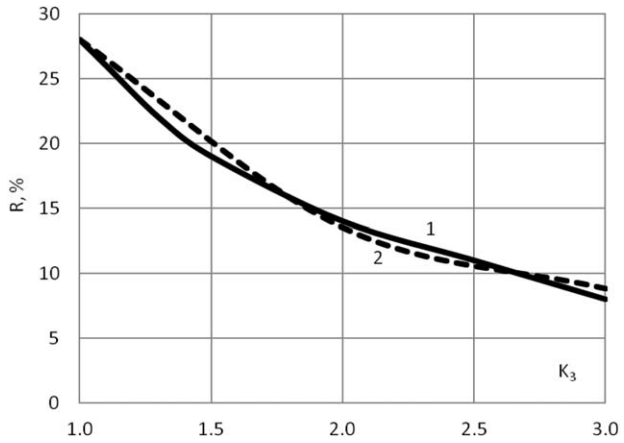

Figure 24. (1) Dependence of the relative difference R on K_3 and (2) approximating function or $R = R(K_3)$.

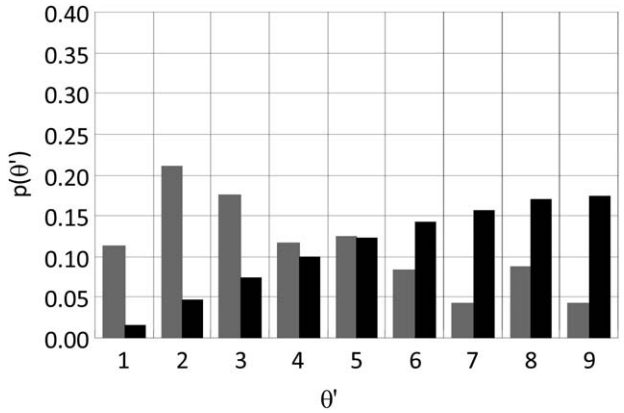

Figure 25. Distribution of struts' angle θ' in Model sample at: (a) K_3 = 1.0 (black) and (b) K_3 = 3.0 (grey).

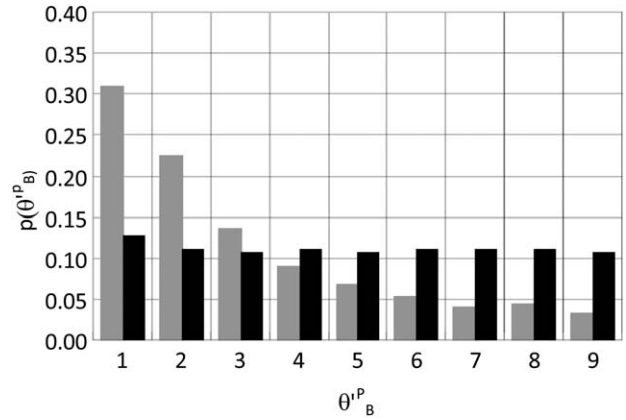

Figure 26. Distribution of struts' angles' projections θ'^{p}_{B} (or θ'^{p}_{C}) in the Model sample at: (a) K_3 = 1.0, isotropic foam (black) and (b) K_3 = 3.0, anisotropic foam (grey); calculation results.

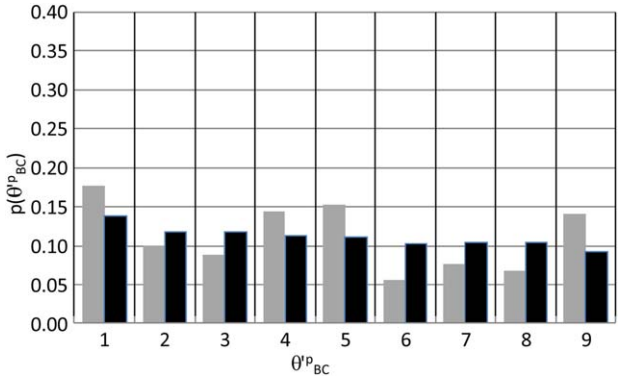

Figure 27. Distribution of struts' angle's projections θ'^{P}_{BC} B + C for experimental specimen 4-2, K_3 =1.10: (a) modelling (black) and (b) experimental results (grey).

2. A mathematical model based on spatially uniform distribution of struts and a linear transformation of coordinates, was elaborated for highly porous transtropic PUR foam ($P > 90\%$) for the determination of the probability density functions of polymeric struts′ length and angles, using experimental data from LM images for finding the parameters. Distribution of struts′ length projections and length themselves fit to a power law with an exponential cutoff, distribution of angles θ' projections—to an exponential law. The histograms of Model sample struts′ angles θ' distribution were constructed and their general trend evaluated.
3. To determine characteristics of transtropic foam 3D strut-like structure, a two-stage procedure was developed, comprising determination of (a) underlying isotropic foam struts′ length distribution function and (b) foam cells elongation degree. A block of PC codes was created and parameters of distribution functions for strut′s length and angles were calculated using experimental data for verification.
4. Several special cases of underlying foam struts′ length probability density distribution were analysed: (a) even, (b) increasing, (c) decreasing, (d) symmetrically triangular, (e) normal, and (f) asymmetric and corresponding distribution functions determined for struts length projections.

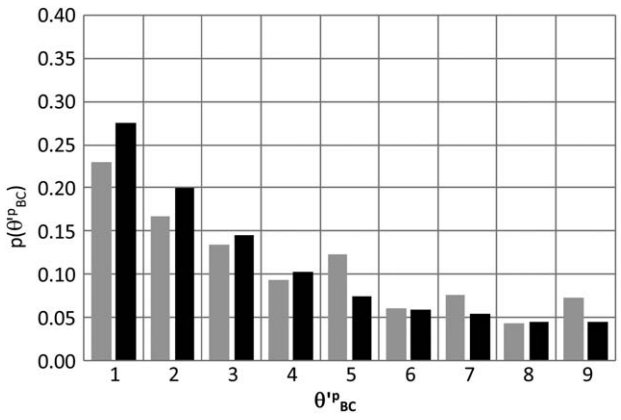

Figure 28. Distribution of angle's θ'^{P} projections θ'^{P}_{BC} on planes B + C for experimental specimen 1-1, K_3 = 2.50: (a) modelling (black) and (b) experimental data (grey).

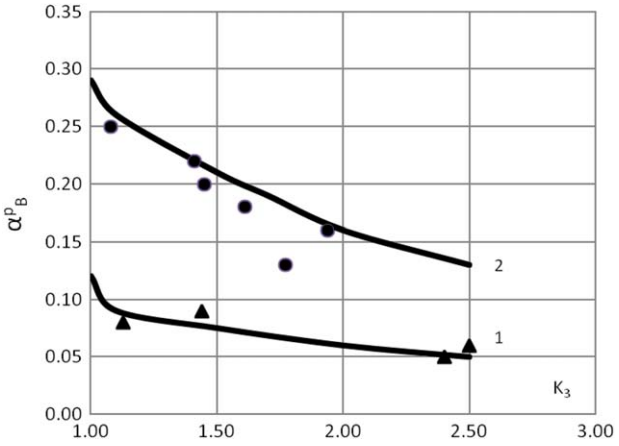

Figure 29. Parameter $\alpha^{P}_{B} = \alpha^{P}_{B}(K_3)$. Theoretical curves: 1 - specimen 1 - 2 and 2 - specimen 5 - 1. Experimental data: ▲- group 1, ● - group 2.

5. A good correspondence of the modelling results with experimental data of five transtropic blocks of highly porous transtropic PUR foam was proved to exist. It was concluded that information on struts′ length distribution was comprised mainly in LM images A having image plane parallel to the plane of isotropy and information on foam cells elongation degree—mainly in images B and C having plane of image perpendicular to it.
6. The differences between the projections and elements themselves (length and angles) were considered for the range of practically most widely occurring elongation degrees of free-rise PUR foam: $1.0 \leq K_3 \leq 3.0$. Numerical calculations revealed that the relative difference between the struts′ average projection′s length on planes B (or C) and average strut length is the biggest for isotropic foam: ≈ 30%. When elongation degree increases to 3.0, the relative difference reduces to 10% and analysis of image B is sufficient for characterization of struts′ length distribution.

The experimental method and mathematical model are directly applicable to characterization of actual spatial strut-like structure of open cell plastic foam: PUR, reticulated polyvinylchloride, cellular rubber as well as natural open-cell materials: sponge, chancellous bone, fiberous materials, etc. The principles of the developed mathematical and computational modelling could be adapted for characterization of 3-D structure of (a) closed-cell plastic foam comprising polymeric platelets instead of struts, (b) orthotropic foam both open- and closed-cell, and

Table X. Orientational Parameter g for Different Models of Spatially Random Distribution of Struts

			g	
N	Model	Sample elements	K_3 = 1.0 (random)	K_3 = 3.0 (oriented)
1	dS_0 = const.	θ'	−0.35	0.30
2		θ' at φ' = 45°	0.00	0.53
3		θ'^{P}_{B} (or θ'^{P}_{C})	0.00	0.53
4	$d\varphi = d\theta$ = const.	θ'	0.00	0.53

(c) short fibers (steel, glass, carbon, etc.) imbedded in a matrix (polymer, concrete, etc.). Further investigations would be performed on structural characterization of orthotropic strut-like structures.

ACKNOWLEDGMENT

The research was performed at EU ERDF project N2010/0290/2DP/2.1.1.1.0/10/APIA/VIAA/053.

AUTHOR CONTRIBUTIONS

Credit for authorship of I.Beverte is based on:

1. a substantial contributions to the research design:
   - literature review,
   - definition of the problem
   - set up of the possible solution
2. the acquisition, analysis or interpretation of data:
   - preparing of the samples for mechanical and microscopic testing
   - development of elements for mechanical testing of samples
   - processing of experimental data
   - drafting and debugging of PC codes
   - numerical calculations
3. drafting the paper
   - composition of text
   - creation of graphs and figures
   - processing the images
   - defining conclusions
4. approval of the submitted and final versions

REFERENCES

1. Berlin, A. A.; Shutov, F. A. Chemistry and Technology of Gas-Filled Highpolymers; Hayka: Moscow, **1980**; p 503 (In Russian).
2. Hilyard, N. C., Ed. Mechanics of Cellular Plastics; MacMillan: New York, **1982**; p 360.
3. Gibson, L. J.; Ashby, M. F. Cellular Solids: Structures and Properties, 2nd ed.; Cambridge University Press: Cambridge, **1997**, p 515.
4. Hawkins, M. C.; O′Toole, B.; Jackovich; D. *J. Cell. Plast.* **2005**, *41*, 267.
5. Mihira, K.; Ohsawa, T.; Nakayama, A. *Koll. Z.,* **1968**, *222*, 135.
6. Michalski, W.J.; Hubeny, H. *Kunststoffe,* **1978**, *68*, 479.
7. Titulaer, R. H. M. The Morphology of Polymer Foams. http://www.mate.tue.nl/mate/pdfs/10724_sec.pdf (accessed December 03, 2012).
8. Hongbin, Sh.; Nutt, S.; Hull, D. *Compos. Sci. Technol.* **2004**, *64*, 2113.
9. Gent, A. N.; Thomas A. G. *J. Appl. Polym. Sci.* **1959**, *1*, 107.
10. Lederman, J. M. *J. Appl. Polym. Sci.* **1971**, *15*, 693.
11. Cunningham, A. *Polymer,* **1981**, *22*, 882.
12. Beverte, I. *Mech. Compos. Mater.*, **1997**, *33*, 719.
13. Lia, K.; Gao, X. -L.; Subhash, G. *J. Mech. Phys. Solids* **2006**, *54*, 783.
14. Lagzdins, A.; Zilaucs, A.; Beverte, I.; Andersons, J. *J. Mech. Compos. Mater.* **2011**, *47*, 1.
15. Lagzdins, A.; Zilaucs, A.; Beverte, I.; Andersons, J. *J. Mech. Compos. Mater.* **2013**, *49*, 1.
16. Stirna, U.; Cabulis, U.; Beverte, I. *J. Cell. Plast.* **2008**, *44*, 139.
17. Beverte, I.; Zilaucs, A. In Book of Abstracts, the 17-th International Conference on Mechanics of Composite Materials, Riga, Latvia, May 28–June 01, **2012**.
18. Beverte, I.; Lagzdins A. In Computational Modelling of Objects Represented in Images: Fundamentals, Methods and Applications III; Giamberardino, P.; Iacovello, D.; Natal Jorge, R. M.; Tavares, J. M. R. S., Eds.; CRC Press: London, **2012**, p 397.
19. Zazhigajev, L. S., Kishjan A. A.; Romanjikov J. I. Methods of Planning and Processing Results of a Physical Experiment; Atomizdat: Moscow, **1978**; p 230 (In Russian).